Retrospective analysis of a non-forecasted rain-on-snow flood in the Alps – a matter of model-limitations or unpredictable nature?

Ole Rössler[1], Paul Froidevaux[2], Uwe Börst[3], Ralph Rickli[4], Olivia Martius[2], and Rolf Weingartner[1]

[1] Oeschger Center for Climate Change Research and Group for Hydrology, Institute of Geography, University of Bern, Switzerland

[2] Oeschger Center for Climate Change Research and Mobiliar Lab for Climate Impact Research and Natural Hazards, Institute of Geography, University of Bern, Switzerland

[3] Department of Geography, University of Bonn, Germany

[4] BKW FMB Energy AG, Bern, Switzerland

Correspondence to: O.Rössler (ole.roessler@giub.unibe.ch)

Abstract

On October 10th, 2011, a rain-on-snow flood occurred in the Bernese Alps, Switzerland, and caused significant damage. As this flood peak was unpredicted by the flood forecast system, questions were raised concerning what has caused this flood and whether it was predictable at all. In this study, we focused on one valley that was heavily hit by the event, the Loetschen valley (160 km^2), and aimed to reconstruct the anatomy of this rain-on-snow flood from the synoptic conditions represented by European Centre for Medium-Range Weather Forecasts' (ECWMF) reanalysis data, and the local meteorology within the valley recorded by an extensive met-station network. In addition, we applied the hydrological model WaSiM-ETH to improve our hydrological process understanding about this event and to demonstrate the predictability of this rain-on-snow flood.

The atmospheric drivers of this rain-on-snow flood were i) sustained snowfall followed by ii) the passage of an atmospheric river bringing warm and moist air towards the Alps Intensive rainfall (average 100 mm /day). It was accompanied by a temperature increase that shifted the zero degree line from 1500 m a.s.l. to 3200 m a.s.l. during 24 h with a maximum increase of 9 K in 9 hours. The south-facing slope of the valley received significantly more precipitation than the north-facing slope, leading to an severe flood in tributaries along the south-facing slope, while the tributaries along the north-facing slope remained nearly unchanged. We hypothesized that the reason for this very local rainfall distribution was a cavity circulation combined with a seeder-feeder-cloud system enhancing local rainfall and snowmelt along the south-facing slope.

Applying and adjusting the hydrological model, we show that both the latent and the sensible heat fluxes were responsible for the flood, and that locally large amounts of precipitation (up to 160 mm rainfall in 12 hours) were necessary to produce the estimated flood peak. With considerable adjustments to the model and meteorological input data, we were able to reproduce the flood peak, demonstrating the ability of the model to reproduce the event. However, driving the optimized model with COSMO-2 forecast data, we still failed to simulate the flood precisely because COSMO-2 forecast data underestimated both the local precipitation peak and the temperature increase. Thus, this rain-on-snow flood was predictable, but requires a special hydrological model set up and extensive and locally precise meteorological input data, especially in terms of precipitation and temperature. Although, this data quality may not be achieved with forecast data, an additional run with an adjusted

58 hydrological model can provide useful information when rain-on-snow events are likely to
59 occur.

60 ## 1 Introduction

61 In the early morning on October 10th, 2011, the discharge of several mountain rivers in the
62 Bernese Alps and the northern Valais Mountains in Switzerland increased very rapidly. In the
63 Loetschen valley, four small tributaries of the main river Lonza rushed to the valley floor,
64 causing erosion and transporting considerable amounts of debris by saturated transport. In
65 addition, extended overland flow was observed at higher elevations. The floods generated a
66 large debris fan at the foot of the south-facing slope, whereas tributaries at the north-facing
67 slope showed no significant runoff. The only road connecting all villages in the Loetschen
68 valley was buried for several hundred meters, and the underlying water reservoir was filled
69 with 200,000 m^3 debris. Fortunately, there were no injuries, but the flood caused total
70 damages of approximately 90 Mio CHF (Andres et al. 2011).

71 Flood predictions using coupled numerical weather predictions (NWP) and deterministic
72 hydrological models are today a standard approach that is further extended using ensemble
73 forecast systems (EPS) to cope with model uncertainties (see review of Cloke and
74 Pappenberger, 2009). In Switzerland, this approach is implemented by combining COSMO
75 and COSMO-LEPS forecast data with an extended HBV hydrological model (Bundesamt für
76 Umwelt, 2009). A dense network of discharge gauging stations is maintained, and the BAFU
77 operationally forecasts the discharge of several river systems. In fact, rising water levels for
78 the river Kander (Bernese Oberland) were predicted for this flood, but the peak on October
79 11th 2011 was strongly underestimated - below the warning level.

80 Shortly after this extreme event, the following questions were raised: a) what exactly caused
81 the flood? and b) why was this event not properly forecasted to warn the public? The
82 authority in charge of hydrological warnings, the Federal Bureau for Environment (BAFU),
83 commissioned a study to analyze the causes of this flood event. The present study is based on
84 a contribution to the BAFU study (Rössler et al. 2013).

85 The flood was preceded by a special weather situation: during the first week of October 2011,
86 a strong high-pressure system brought a period of warm and clear weather to the Swiss Alps.
87 These stable weather conditions were replaced by an extratropical cyclone on October 7th that
88 led to extensive snow fall down to 1,200 m a.s.l. The snow fall lasted until October 9th. After

89 some hours of sunshine on October 9th (hereafter 9 Oct.), a warm front reached the Alps from
90 the North West in the early morning on October 10th (hereafter 10 Oct.) and triggered heavy
91 rainfall locally. The flood was hence a typical rain-on-snow event.

92 Rain-on-snow floods are known as one of five flood types occurring in temperate climate
93 mountain river systems (Merz and Blöschl 2003). While most studies about rain-on-snow
94 events have been done in North America, this flood type is also reported from Europe (e.g.
95 Sui and Koehler 2001), Japan (Whitaker and Sugiyama 2005), and New Zealand (Conway
96 2004). Characteristically, the rain is partially stored in the snow cover up to the liquid water
97 holding capacity (~10.0% snow water equivalent (SWE) of the snow water) and is later
98 released from the snow cover. The melting energy from the liquid precipitation causes
99 enhanced direct runoff that is due to both increased snowmelt and decreasing water holding
100 capacity; hence, more water is released from the snow. The snow cover can therefore be an
101 amplifying factor for floods, or it can have a curbing effect, if the snow cover is too thick or
102 the melting energy too low.

103 According to McCabe et al. (2007), the main driving factors for a rain-on-snow flooding are
104 the extent of the snow-covered area, the freezing and thawing elevations, the water equivalent
105 of the snow cover, and the liquid precipitation amount. Merz and Blöschl (2003) also stress
106 the importance of latent heat input and point to the occurrence of extended overland flow
107 during rain-on-snow-events because soils are saturated by antecedent snowmelt processes.

108 In general, the prediction of floods remains challenging as small differences in precipitation
109 and temperature cause strong biases in the hydrological prediction, especially in mountainous
110 areas with small response times, and the sensitive effect of the snow limit determination on
111 runoff (Jasper et al., 2002). The prediction of rain-on-snow events is even more challenging as
112 it requires accurate information on snow covered area and snow water equivalent. McCabe et
113 al. (2007) stated that the prediction of rain-on-snow events is not only limited by the
114 meteorological input parameter, but also by insufficient knowledge about the important
115 processes involved. The latter is even more valid for Europe with far less research attention
116 on rain-no-snow events, than for instance in North America. Hence, data of observed rain-on-
117 snow events and case studies revealing in detail the causes and process-sequences of this
118 important and fascinating hydro-meteorological process is required to improve our process
119 understanding and to improve the forecastability of such extreme events.

Due to the hydro-meteorological character to this rain-on-snow-flood in the Loetschen valley, we chose a comprehensive approach by aiming to reconstruct the flood anatomy starting from the synoptic-scale conditions down to the local observations. First, to broaden our current process-understanding of rain-on-snow floods, we want to elucidate the relevant synoptically and locally observed processes behind this event and to compare them with the key processes of typical rain-on-snow events. Second, to estimate the predictability of the rain-on-snow flood, we applied a hydrological model (WaSiM-ETH) to evaluate its ability to reproduce the local flooding. Third, we assessed the predictability of the rain-on-snow flood by driving the hydrological with COSMO-2 forecast data. This will lead to a final assessment of past and future predictability of such rain-on-snow events.

2 Materials and Methods

2.1 Study Area

The Loetschen valley lies just south of the Bernese Alps, which acts as the first barrier for the predominantly northwestern atmospheric inflows. As a result, the highest annual precipitation amounts in Switzerland are found within this mountain range (Jungfrau, Eiger, Mönch, >3,600 mm per year, Kirchhofer and Sevruk, 2010). The Loetschen valley is situated in the transition zone between this area of highest precipitation amounts and the driest region in Switzerland (Rhone valley, Stalden, 535 mm per year). The valley (Figure 1) stretches from 600 m at the southern outlet up to approximately 4000 m a.s.l., with a mean elevation of 1,800 m a.s.l. The valley bottom extends from the southwest to the northeast and rises slightly from approximately 1,200 m a.s.l. to 2,100 m a.s.l. at the glacier tongue; all of the surrounding mountain ridges are approximately 3,000 m a.s.l., and the mountain tops are higher. Dominant vegetation types are coniferous mountain forests and alpine pastures. Nearly 18 % of the catchment is glaciated. The Lonza is the main river in the valley and is fed by numerous small tributary rivers from the north- and south-facing slopes and the highest elevations. The black arrows in Figure 1 mark the rivers that had extraordinary floods during the October event (from left to right: Ferdenbach, Milibach, Tännbach, and Gisentella). Notably, none of the rivers on the north-facing slope showed any extreme flooding.

2.2 Methods for reconstructing the flood

2.2.1 Reanalysis and soundings data

The four day synoptic evolution preceding the event is analyzed using the Era-Interim-reanalysis dataset from the European Center for Medium-Range Weather Forecasts (ECMWF) (Dee et al., 2011). This reanalysis dataset results from a numerical weather prediction model frozen in time that is continuously forced by a complex assimilation of various observations of the atmosphere, ocean, and land surface. It is commonly used for the retrospective analysis of meteorological situations. The main atmospheric variables are available on a three dimensional grid (T255 horizontal resolution, interpolated to a 1 x 1° grid, 90 vertical layers) every six hours. In addition to these gridded data, vertical characteristics of the atmosphere recorded from weather balloons launched in Payerne (cp. Figure 1) were analyzed. The Payerne upper air soundings station is located in the Swiss Plateau 80 km northwest of the Loetschen valley (upstream of the investigated flood event, see Figure 1). These weather balloons are launched twice a day and provide high resolution profiles of temperature, humidity, wind velocity, wind direction and pressure. Here, we compared radio-sounding data from the day before (9 Oct. 00 UTC) with data from the day of the flood event (10 Oct. 00 UTC).

2.2.2 Local meteorological observations

The local development of the hydro-meteorological event is analyzed in detail using data from a dense network of observations in the Loetschen valley. The Lonza river discharge is officially measured by the BAFU at the center of the valley (Blatten gauge, Figure 1), and inflow to the reservoir of the EnAlpin hydropower was provided by the operating company for the event period (Ferden reservoir gauge, Figure 1). Eight meteorological stations are distributed in the valley. These stations are located on both sides of the valley at different elevations. Two stations are operated by the Institute for Snow and Avalanche Research (SLF), and one is operated by a private weather service, MeteoMedia. All other stations were set up by the Department of Geography, University of Bonn (GIUB) during a previous research project (Börst, 2005, cp. Table 1). This high network density enables a very detailed analysis of the meteorological conditions in the valley during the rain-on-snow-event. The meteorological stations are equipped with standard measuring devices for temperature, precipitation, air humidity, wind speed, wind direction, global radiation, and snow depth.

Table 1 summarizes the location and equipment at each station; IDs refer to the numbers in Figure 1. All rain gauges are unheated; therefore, precipitation depth and duration during snow fall and in the transition from snow to rainfall must be analyzed with caution.

2.2.3 Hydrological Modeling

The retrospective modeling of the flood was conducted using the WaSiM-ETH distributed hydrological model. This physically based, fully distributed model has been successfully applied to several alpine catchments and research questions (Verbunt et al., 2003, Rössler et al., 2012). Rössler and Löffler (2010) demonstrated the ability of this model to reproduce the water balance and runoff in the Loetschen valley. Basically, WaSiM-ETH solves the water balance equation for each raster cell using physically based equations; for example, infiltration is calculated using the Green and Ampt (1911) approach, and water fluxes within the unsaturated zone are based on the Richards equation. Lateral fluxes are less adequately reproduced; interflow is generated at each raster cell; however, the interflow is not routed to the underlying raster cell, but rather, it is directly assigned to the nearest drainage channel with a topography-derived travel-time delay. Surface runoff, interflow, and base flow are superposed for runoff generation, and runoff concentration is described by conceptual recession parameters that refer to the response time of a catchment after rainfall. These recession constants are used for direct runoff (kd) and interflow (ki) and need to be derived from the hydrograph or need to be calibrated (Hölzel et al. 2011). WaSiM-ETH requires spatial data of soil and land use types and a digital elevation model. The characteristics of the two former data sets must be parameterized according to the assigned types (e.g., soil hydraulic properties, soil magnitude, root depth, and leaf area index). Meteorological information for each raster cell is generated by interpolating meteorological point data to the entire catchment, which can be achieved in several ways. The simplest methods are the Thiessen polygon (TP) interpolation and the inverse distance weighting (IDW) methods; these methods depend solely on the spatial distribution of the meteorological stations. A more advanced method is the combination of IDW with an elevation-dependent regression (IDWREG). Elevation-dependent regression can be useful in areas with high elevation gradients, such as the Loetschen valley. In addition, WaSiM-ETH is able to make use of externally processed data, such as the COSMO forecast data sets. All of these methods are described in more detail by Schulla (2013). As the focus of this study is the simulation of a rain-on-snow-event, the reproduction of snowmelt is crucial. In WaSiM-ETH, different

methods can be applied. The standard technique is a degree-day-factor-model (hereafter called SM1) that simply multiplies a degree-day-factor (C0) with the temperature above the temperature of snowmelt (T0). In addition, WaSiM-ETH offers the possibility to consider latent heat fluxes as they occur during rain-on-snow events using an energy balance model after Anderson (1973) (hereafter called SM2). For precipitation sums of more than 2 mm/day, the SM2 approach calculates the snowmelt as a function of sensible heat (degree-day-factors (C1, C2) considering wind speed, (C1 + C2 * windspeed) * snowmelt temperature), latent heat considering saturation deficit, (C1 + C2 * windspeed) * saturation vapor pressure – 6.11), radiation melt (1.2 * air-temperature), and energy from liquid precipitation (0.0125 * precipitation * air-temperature) (cp. Schulla, 2013). The factor in the latter equation represents the heat transfer of rainfall water into the snow and is defined solely as the heat capacity of one degree Celsius water (4.184 J/g) divided by melting energy of snow (333.5 J/g). When the precipitation amount during one time step is less than 2 mm, melt is calculated using the simple degree-day-factor model (SM1). In addition, the SM2 also subdivides the snow cover into a liquid and a solid part and the maximum water holding capacity has to be parameterized (standard 10%, Schulla, 2012). In both model versions the water from snowmelt and rainfall percolates without delay through the snow cover and infiltrates into the soil. To account for lateral processes in the snow cover, a fraction of this water is directly attributed to surface runoff (parameter SF). This fraction needs to be calibrated.

To analyze the key processes causing the flood, we applied a previously calibrated model version (Rössler and Löffler, 2010) in a recent version of WaSiM-ETH (version 9.2, Schulla 2013). The model has a temporal resolution of one hour and a spatial resolution of 50 x 50 m. It was calibrated against discharge for the year 2002 and validated for 2003-2007. Statistical measures such as the Nash-Sutcliffe-Index (cal.: 0.84, val.: 0.8), Pearsons-R (cal.: 0.94, val.: 0.95) and the Index of Agreement (cal.: 0.96, val.: 0.95), in addition to the water balance, demonstrated the model's ability to reproduce discharge from the Lonza catchment (Rössler and Löffler, 2010).

2.2.4 Stepwise adjustments of the standard hydrological model

The hydrological modeling should not be understood as an end in itself but as a tool to improve the process understanding and the forecast. The former is especially the case if models are not consistent with the observations (Beven, 2001). Hence, in this study, we wanted to determine which parameters, algorithms and data sets must be adjusted to simulate

this rain-on-snow-flood. We used the previously calibrated model as a starting point, and we gradually changed the model to represent the flood peak in the Lonza River during this event. Each gradual change is underpinned by hypothetical assumptions of the underlying processes to reach a better understanding of the processes involved. Changes are made to input data sets, single model algorithms, and parameter values.

1. Model parameter adjustments

In the course of this study, three model parameters ("fraction of direct flow from snowmelt" (SF), "runtime of direct flow (kd) and interflow (ki)", and the melt-factors of the snow-modules (C0, C1, C2)) were adjusted to account for deviations between the modeled and the observed discharge. All model parameters for the standard model set up as well as the adjusted values of all model versions used, are summarized in Table 2. The "fraction of direct flow from snowmelt" (SF) defines the proportion of liquid water in the snow cover that infiltrates into the soils and the proportion that is directly assigned to surface runoff. In this study, we increased this value considerably (from 10% to 90%) under the assumption that the soil below the snow cover was saturated very quickly and directly cause surface runoff. Although this adjustment was necessary to fit the model to the observed runoff, the increased value is quite high and therefore unlikely, but still possible. For the same reasons, we decreased the "response times of direct flow and interflow" that indicate the response time to precipitation events in the catchment. These parameters are typically derived from a hydrograph if observations are available.

Finally, melt factors determine the amount of water that is melted per time step and the energy available (latent and sensible). The melt factors were adjusted with respect to both discharge and snow water equivalent by comparing model output with observed runoff at Lonza (Ferden) and observed snow water equivalent at the SLF station Gandegg (2,717 m a.s.l.). Observed SWE is derived from measured snow depth, assuming a snow density of 0.1 g/cm^3 for newly fallen snow. Accordingly, derived observed SWE was compared only with the modeled solid part of the snow cover. Nevertheless, snow density is very sensitive to the validation of the modeled SWE: According to Judson and Doesken (2000) snow density can range from 0.05 g/cm^3 to 0.35 g/cm^3; Jonas et al. (2013) assumed for the same rain-on-snow event a value of 0.15 g/cm^3; and an equation recommended by Pomeroy et al. (1998) for fresh snow suggests 0.071 g/cm^3. In addition, during the rain-on-snow event the density is likely to increase due to compaction by wind and rainfall, and higher liquid water content. As no data

about density development were available, we assumed a constant value throughout the event but considered an uncertainty range of +/- 25 % (0.075 – 0.125 g/ cm^3). The modelling of the snow dynamic was validated at all further stations in the Lötschen valley.

2. Changing the snow module in WaSiM-ETH

We used two of the four different snow modules available in WaSiM-ETH. First, we applied the simple but straightforward degree-day-approach (SM1). Second, a snowmelt model was used that considers not only the sensible heat (temperature) as the degree-day-module does but also the latent energy (SM2). The performance of these modules indicates whether sensible heat alone or a combination of latent and sensible heat controls snowmelt and runoff generation.

3. Input data sets

Precipitation is a crucial input data set; accordingly, the applied regionalization approach and the chosen meteorological stations determine the modeling results. Initially, we used the IDWREG approach based on the same official meteorological stations as used in the first calibration and added one additional station (Gandegg, Figure 1) situated directly within the most affected catchment Milibach. Subsequently, we used a refined data set that incorporates all official (see Figure 1) and all private meteorological stations available (see Table 1), despite their inaccuracies in recording solid versus liquid precipitation. Snow fall measurements from the SLF station Gandegg was found to be more accurate compared to snow measurements from private stations. Hence, we fitted the precipitation against snow depths (assuming a density of 0.1 g/cm^3) measured at the SLF IMIS station Gandegg. This resulted in a correction factor of 0.85 for snow fall. In terms of liquid precipitation an overestimation is likely as this measured rainfall is biased by the snow in the rain gauge. Here, we also applied a reduction of 15% (up to 24 mm). As this procedure is quite uncertain, we evaluated these corrections against discharge and snow measurements from all private stations, and found the best performance using this correction.

2.2.5 Test of the event predictability

To test the predictability of the event, we applied the optimized model that reproduced the flood peak best and used the COSMO-2 forecast model data (Meteoschweiz, 2010) as meteorological input data. COSMO-2 is a high-resolution numerical weather forecast model

with a spatial resolution of 2.2 x 2.2 km. It is used by several meteorological services in Europe; in Switzerland, it is applied in combination with the coarser resolution COSMO-7 model. COSMO-2 is updated eight times a day and provides a forecast of 24 hours. Here, we used COSMO-2 temperature and precipitation data from 18 h, 12 h, and 6 h in advance of the flood peak on Monday, 10 Oct. 12 UTC, 2011.

3 Results

3.1 Precursor weather conditions

The weather conditions in the Loetschen valley between 7 Oct. and 10 Oct. first changed from warm, dry, and bright conditions to cold temperatures and snowfall on 7 Oct. (minus 14 K from 6 Oct. 11 UTC to 7 Oct. 11 UTC, ECMWF data), and then changed back to warm conditions with significant amounts of liquid precipitation on 10 Oct. (plus 9 K and more than 100 mm of rain locally, ECMWF data). The following large-scale atmospheric flow evolution was responsible for these rapid changes in temperature and precipitation:

A coldfront associated with a low pressure system over Scandinavia led to a distinct temperature contrast across the Swiss Alps on Friday 7 Oct. 2011 (Figure 2 a). After the frontal passage, a northwesterly flow of polar air brought snowfall on Saturday 8 Oct. (Figure 2 b). The temperature at 850 hPa was close to zero, and the snowfall limit was located at approximately 1500 m a.s.l. On Sunday 9 Oct. (Figure 2c), the northwesterly flow weakened, and around midnight, a warm front associated with a low pressure system over Iceland reached Switzerland from the northwest. This warm front was of crucial importance for the flooding for two reasons. First, it was accompanied by a rapid rise of the temperature of 9 K in 24 hours between 9 Oct. 06 UTC and 10 Oct. 06 UTC. Second, it was followed by a very strong northwesterly flow bringing warm and remarkably moist air into the Alps. . Figure 2 d-f shows with arrows the wind at 850 hPa, with blue shadings the vertically integrated precipitable water (here the moisture and the cloud water) over the whole troposphere and with a violet line the areas where strong wind a high precipitable water are combined. The red line delimits the dynamical tropopause and will be discussed later. The Figure clearly shows that the warm front was located at the head of a narrow band of moist air spreading across a large area over the Atlantic. The trajectory of this moist air along a low level jet and around the Azores anticyclone is depicted in Figure 2 d-f. This moist band fulfilled the characteristics

of an atmospheric river (AR, violet contour line in Figure 2 d-f) as defined by Ralph and Dettinger (2011). The vertically integrated precipitable water exceeded 20 mm, wind speed in the lowest two kilometers was greater than 12.5 m/s, it was a few hundred kilometers wide and it extended for thousands of kilometers across the North Atlantic (Figure 2 d-f).

Comparing the event with all October data in Era-Interim at the grid point upstream of the Loetschental (47°N, 7°E), we found that negative temperatures at 850 hPa occurred approximately 3 days per month in October during the 33 years considered. The warm temperature on the 10 Oct. was not unusual neither (approximately found 9 days per month). In contrast, a temperature rise of 9.0 K in 24 hours is rare, such a rise occurred only 12 times in October in the last 33 years. We also computed the integrated moisture transport and found that the amount of moisture transported towards the Alps (from a north-north-westerly direction) was exceptional. The time steps of 10 Oct. 00, 06, and 12 UTC, which correspond to the arrival of the AR in the Alps and to the time of intense rainfall, are among the 6 time instances with the highest fluxes of moisture upon the orography during the whole Era-Interim period and over all months. The passage of the cold and the warm fronts at the surface was associated with the passage of a high potential vorticity (PV) trough, or positive PV anomaly, at the tropopause level. The evolution of the tropopause level flow is illustrated using the dynamical tropopause on the 325 K isentropic surface (Figure 2 d-f, red line). The dynamical tropopause is co-located with the jet. Positive upper level PV anomalies influence the structure of the atmosphere underneath them, such that colder air and reduced stability are typically found below (e.g., Schlemmer et al., 2010). The red line in Figures 2 d, e, and f show the subsequent development of the PV anomaly. The excursion of polar air towards the equator is located below the positive PV anomaly and the passing of the cold and warm fronts corresponds to the upstream and downstream flanks of the trough, respectively. A more general statement is that the passage of a trough followed by the passage of a ridge and the associated major variations of upper level PV must coincide with important changes in stability, vorticity and temperature in the mid to low troposphere. Such rapid and intense changes of the flow properties over areas as large as the alpine range must coincide with the meridional transport of air masses and abrupt air mass transitions.

The vertical extent of the change from cold and dry to warm and wet atmospheric conditions was captured by the upper air soundings launched in Payerne at 00 UTC on 9 Oct. and 10 Oct. (Figure 3). The comparison of the two profiles shows that the freezing level rose from 1,500

to 3,000 m a.s.l. in 24 hours. This strong warming was associated with a remarkable moistening as depicted by the concomitant rise of the zero-degree dew point temperature from approximately 1,500 to 3,000 m a.s.l. In the profile from 10 Oct., two different air masses can be distinguished: A very stable (isothermic) and cold layer extended from the surface up to 800 hPa on top of which a less stable layer extended over the whole tropopause. This points to flow blocking along the northern face of the Alps at the time of the warm front arrival. The low-level cold pool might have played a role in determining the distribution of precipitation by pre-lifting the air and by creating a level of wind shear (between the retarded blocked flow and the fast unblocked flow). Strong shear can favor the development of turbulent cells embedded in a cloud layer and associated up- and downdrafts, which in turn might influence precipitation growth mechanisms significantly (see, for example, Houze and Medina, 2005). The wind direction (not shown) was mostly NW to N from 2,000 m upwards.

That the air was lifted over the Alps rather than being blocked by the Alpine barrier can be determined from the Froude number (F) (Reinecke and Durran, 2008). F is the ratio between the kinetic energy of the wind and the energy required to pass over a barrier. If F is larger than 1, the air can surpass the Alpine barrier. F was > 1 from 2,200 m upwards (not shown), indicating that the air masses located approximately 2,200 m a.s.l. above Payerne were flowing over the Alps, resulting in a North Foehn condition. Values of F < 1 below 2,200 m a.s.l. confirm the presence of a blocked cold air pool near the surface.

It is interesting to compare the temperature profiles retrieved from the upper air sounding with the 2-meter temperature profiles of the Loetschen valley retrieved from surface thermometers (Figure 3). While the vertical profiles are very similar on 9 Oct. 00 UTC, the valley floor is significantly cooler than the free air on 10 Oct. 00 UTC. This difference might be the result of the intense snowmelt during the passage of the warm front. Snowmelt requires significant energy input from the surface air and evidence for it is given later by station measurements. The soundings themselves also show that large scale conditions were very suitable for widespread and intense snowmelt. Both the temperature and the dew point temperature reached positive values up to 3,000 m a.s.l. A positive dew point temperature is very important for snowmelt. If air with a positive dew point temperature is in contact with snow, and hence cooled to 0° C, it will be oversaturated and condensation will set in. Each gram of condensed water vapor releases sufficient energy to melt 7 grams of snow; therefore,

401 snowmelt will be significantly enhanced by latent heat transfer adding to sensible heat transfer
402 from the air into the snow.

403 In summary, the following large-scale atmospheric ingredients led to the flood in
404 Loetschental: A precipitation-triggering cold front led to several decimeters of fresh snow
405 down to a relatively low altitude compared to the October climatology. This situation would
406 have been harmless, however, without a rise of the snow line of a rare rapidity and the sudden
407 arrival of warm and moist air (AR) from the North West on the evening of 9 Oct. The AR
408 resulted in an exceptionally intense transport of moisture towards the Alps and significant
409 amounts of rainfall on 10 Oct. over the freshly snow-covered areas.

410 ## 3.2 Local meteorological conditions

411 Eight stations distributed throughout the Loetschen valley confirmed the course of the general
412 weather conditions previously described. Figure 4a-d summarizes the development of the 2-
413 meter air temperature (Figure 4a), the relatively humidity (Figure 4b), the accumulated liquid
414 (Figure 4c), and the solid precipitation (Figure 4d) from 7 Oct. to 10 Oct. at each station. A
415 strong cooling occurred on the 7 Oct. and negative temperatures where recorded down to
416 1,470 m a.s.l. (Ried) on the 8 Oct. and early 9 Oct., confirming that the snow limit was
417 situated at approximately 1,500 m. Only the Wiler station, at 1,415 m, experienced slightly
418 positive temperatures. On 9 Oct., the stations at the valley bottom recorded a diurnal
419 temperature increase of up to 9 K, which might indicate an intermediate period of clear sky.
420 In contrast, no significant diurnal temperature cycle was recorded at higher elevations.
421 Between 9 Oct. in the evening and the morning of 10 Oct., a rapid warming was recorded at
422 all stations (+9 K). The zero-degree-line was found around 1,500 m a.s.l. (Wiler) before and
423 around 3,200 m a.s.l. during the event (Sackhorn). This warming coincided with the arrival of
424 the warm front and was most pronounced close to the Northern crest, at the Sackhorn and
425 Gandegg stations (cp. Figure 1).

426 The temporal evolution of liquid (Figure 4c) and solid (Figure 4d) precipitation was similar at
427 all stations, but the recorded precipitation amounts varied significantly. Rainfall amounts
428 generally increased with altitude and, interestingly, significantly more rain fell on the south-
429 facing slope than on the north-facing slope. For example, the Chumme station recorded more
430 than twice as much precipitation (108 mm) than the Mannlich station (42 mm) at the same
431 elevation on the opposite slope. The small scale wind field that caused this rainfall pattern

will be discussed at the end of this section. The highest precipitation amounts at the valley bottom were found near Wiler; precipitation first decreased going eastward (Ried) before increasing with increasing elevation (comparing Wiler – Ried – Grund – GrossiTola). Snow depth was more linearly correlated to altitude than rainfall, with snowfall starting earlier, lasting longer and being more intensive at higher elevations. For example, the snow amounts recorded at Chumme and Mannlich are similar. Evidence for snowmelt is given by the rapid decrease of snow depths, amounting to 40 cm at Chumme and Mannlich and 60 cm at Gandegg in six hours in the morning of 10 Oct. The onset of snowmelt is delayed by several hours going from 1,900 m (Grund) to 2,200 m (Chumme and Mannlich) to 2,700 m (Gandegg) because of lower temperatures at higher elevations. Minor snow accumulation is also recorded at Ried (1,470 m a.s.l.) with a maximum of 10 cm. A slight ablation is also visible. A more exact estimation of the snow cover dynamic is not possible due to the measurement uncertainties. Those uncertainties are expressed in the strong and short fluctuations visible in all snow depth curves and stem from wind drift, movements of the underlying grass, shrinking and swelling of the soil, and freeze-thaw processes. Figure 5 shows wind directions recorded on 10 Oct. at 8 stations inside the Loetschental valley. The diagrams indicate the numbers of measurements (relative frequency) from each direction. Sackhorn station (located at the valley crest) is the only one recording a high frequency of NW wind consistent with the synoptic scale flow (the wind blowed exclusively from a WNW to NW direction). It is the only station directly exposed to the incoming synoptic wind from the NW. All of the other stations, located on northern flank of the valley, i.e., the lee side of the Northern crest, registered local circulations inside the valley. Ried, Grund and Grossi Tola stations along the WSW-ENE valley axis recorded along-valley winds with a predominance of wind in the downslope direction. At Wiler, the wind direction was highly variable. Both mid-slope stations, Chumme and Mannlich, show wind directions similar to those at the valley bottom. Particularly interesting is the Gandegg station, which is the only one recording a SE wind. Remarkably, the wind direction at Gandegg was opposite to the wind direction at Sackhorn, which located only 1.3 km away.

The large scale analysis showed that the synoptic situation was conductive to a rain-on-snow event with the successive passage of two precipitation-producing fronts, a rapid rise of the snow line and exceptional amounts of moisture transported towards the Alps. In addition to the synoptic forcing, the dense network of meteorological stations points to strong variations

at the local scale. The rain-on-snow event was intense close to the northern crest (10 K temperature increase in 12 hours, 160 mm of rain in 6 hours and a snow depth decrease of 60 cm in 12 hours at Gandegg) and gradually less intense from north to south across the valley. Rainfall totals decreased by a factor of 4 along a 6 km cross section between Gandegg and Mannlich. This remarkably steep rainfall gradient indicates kilometer-scale heterogeneity of the atmospheric flow.

The interaction of the synoptic scale atmospheric flow with the complex alpine topography can trigger local extreme weather via many different processes. We postulate that the development of a so-called cavity circulation in the lee of the northern crest (see Figure 6) might have led to the observed rainfall gradient. A second cavity circulation might have occurred also in the lee of the southern crest, but this remains speculative due to missing data (question mark, Figure 6). Cavity circulations are rather frequent in the Northern Alps and often captured by webcams. Typically, they are recognized through the formation of so-called banner clouds (see for example Wirth et al., 2012). We have no proof of a cavity circulation early on 10 Oct., but some evidence points towards its probable occurrence. First, the wind directions recorded at Gandegg were upslope, i.e. opposite to the background wind. Second, relative humidity indicated the occurrence of a surface cloud along the upper southward facing slope. Third, the Froude number was much larger than unity, indicating the presence of "flow over" conditions necessary for the formation of gravity circulation. A cavity circulation implies upslope ascent on the lee side of the mountain crest as shown in Fig. 6. Such an upslope ascent and the associated adiabatic cooling, saturation, and cloud formation at low levels, can enhance snowmelt very efficiently through sensible and latent heat transfer to the snow. Rainfall can also be enhanced significantly by low level clouds through the seeder-feeder effect. Indeed, in the case of low level clouds, the hydrometeors created higher above by the seeder cloud fall through a saturated layer and are not evaporated. Moreover, they collide with the low level droplets so that rainfall efficiency can rise significantly. Forced ascent from the topography and saturated air is likely to have produced a low level cloud on the windward side of the northern crest as well; therefore, intense snowmelt and intense precipitation is likely to have occurred on both sides of the Loetschen valley's northern crest. There is unfortunately no measurement station on the windward side, but flooding, landslides, and damages have been reported from the Gasteren valley, which contributed to the 100 year flood event in the Kander valley.

The rapid decrease of snow depth as measured at the Gandegg station might be interpreted as either efficient snowmelt accelerated by high surface water vapor and/or snowpack melt and compaction by locally enhanced rainfall. The rain was most likely stored in the fresh snowpack until saturation was reached. Additionally, the snowpack not only acted as a runoff enhancer by trapping and releasing the rainfall water, but also by contributing a considerable amount of snowmelt water to the runoff.

3.3 Retrospective modeling of the event

To gain more knowledge about the involved processes and flood predictability, we retrospectively modeled the event, based on a previously calibrated version of the model. First, we simulated the flood discharge at two gauges, Lonza-Blatten (BAFU) and Lonza-Ferden (EnAlpin), to validate the performance of both the initial model and the adjusted model. In a second step, modeled discharge was evaluated for the ungauged tributary river of the Lonza at the southern slope, Milibach, affected by the highest precipitation amounts and flooding (estimated 32 m^3/s, unpublished data, Geoplan Naturgefahren).

Figure 7 comprehensively illustrates the modeled temperature, precipitation and the resulting simulated and observed discharge for Lonza at Blatten and Ferden during the period of interest for standard and refined meteorology. At first, we focus on the standard meteorology: The temperature shows clear diurnal variations between 1 Oct. and 6 Oct. Then, along with a rapid temperature decrease, snow began to fall and continues to fall constantly for two and a half days. Intense rainfall accompanied by temperatures rising to positive values starts after a short period of dry conditions. The observed runoff corresponds to these weather conditions, with diurnal runoff cycles of glacier melt followed by constant base flow during the cold period and an abrupt rise in flow around noon on 10 Oct. Observations from Lonza at Ferden are missing after 10 Oct. 12 UTC due to damages at the gauge. The recorded 123 m^3/s are assumed as the flood peak, although this remains uncertain.

Using the hydrological model calibrated in a previous study for mean-flow representation (Figure 7, left, blue line), the general sequence of the runoff is reproduced, but the flood-peak on 10 Oct. is strongly underestimated, especially for the Lonza at Ferden (Lonza, Blatten: 42 m^3/s modeled, 64 m^3/s observed; Lonza, Ferden: 60 m^3/s modeled, 123 m^3/s observed).

Therefore, two different peak-optimized model versions were set up to reproduce the flood maximum for Lonza at Blatten and Lonza at Ferden with increasing degrees of deviation from

527 the standard model. One model version was obtained by adjusting only one model parameter
528 (green line, Figure 7, left) using SM1 under standard meteorology: the fraction of snowmelt
529 that is directly routed to the drainage without infiltration (SF) was increased from 10% to
530 90%. In the second model version (orange line, Figure 7), we used SM2, which extends the
531 sensible heat determined by the degree-day approach by incorporating the latent heat transfer
532 from precipitation, radiation, wind, and humidity. Both model versions show a much better
533 representation of the flood peak and are able to reproduce the flood for the Lonza at Blatten,
534 while underestimating the flood at the underlying gauge for the Lonza, Ferden.

535 An additional third model version used refined meteorology from our meteorological station
536 network for the model inputs and adjusted parameters for the snow (SM2 approach) and
537 routing modules (magenta line, Figure 7, right); the model parameters were adjusted to
538 simulate the Milibach catchment flood peak (see below). This model version is able to
539 reproduce both flood peaks, but overestimated runoff in the days before the event. The
540 standard hydrological model using SM1 under refined meteorology simulated at flood peak of
541 only 75 m^3/s. Thus, the hydrological model adjustments were more relevant than the refined
542 meteorology to achieve a good representation of the flood peak. This refined meteorology was
543 generated as follows:

544 Local observations indicated a strong heterogeneous distribution of liquid precipitation with a
545 focus on the northern rim of the valley (see the section on local meteorology). Comparing
546 these observations with the modeled precipitation distribution, the standard model
547 regionalization - based on official meteorological stations and the Gandegg station - had a
548 homogenous, strongly height-dependent precipitation pattern (Figure 8, upper panel, standard
549 meteorology) with miner valley intern variations. Accordingly, the precipitation sums on the
550 north-facing slope are overestimated (110 mm modeled vs. 42 mmm measure at Mannlich, cp.
551 Figure 4d) and those on the south-facing slope are underestimated. We refined the
552 interpolation by including all of the meteorological stations available, and we specified a
553 mainly southwest-northeast precipitation field to correspond with the topography of the valley
554 (Figure 8, lower panel, refined meteorology). The resulting liquid precipitation distribution is
555 closer to that described in the local meteorology section.

556 The effect of this refined meteorology is analyzed using the model performance in the
557 Milibach tributary catchment. Figure 9 shows the modeled and observed runoff as well as
558 weather and snow depth at the Gandegg meteorological station, which is located within the

559 Milibach catchment. The left panel summarizes the performance for the standard meteorology
560 with both snowmelt algorithms (SM1 and SM2) applied, while the right panel shows the
561 model output for the SM2 melting using the refined meteorology. For the latter, we also
562 adjusted the snowmelt parameters to reproduce the snow cover depletion correctly. As the
563 reference, we used observed snow depth at Gandegg that was converted into SWE by
564 assuming a constant snow density of 0.1 g/cm^3 with uncertainty bands of +/- 25%.

565 Under standard meteorology and standard parameter setting, the SM1 approach is not able to
566 melt the snow cover, because energy input from sensible heat (temperature) was too low at
567 this elevation. Using the SM2 approach, snow is melted, but both snow accumulation and
568 snowmelt were overestimated. These limitations were removed in the adjusted model version
569 under refined meteorology. In addition, we increased the water holding capacity from 10% to
570 20% of SWE to account for overestimations of discharge at gauges in Blatten and Ferden.
571 Under both SM2 approaches and both water holding capacities, the snow is saturated after the
572 first rainfalls shortly after midnight on 10 Oct. To ensure that the modeled snow dynamic is
573 also correct in the other parts of the valley, we compared the modelled SWE with SWE
574 derived from snow height observation (Figure 4d). Figure 10 illustrates the snow
575 accumulation and snowmelt for all three model versions at four different stations in the
576 Lötschen valley. It proves that the adjusted hydrological model using SM2 and refined
577 meteorology (light green line) is able to simulate the snow dynamics in general in the entire
578 valley. Smaller differences occur at the south-facing slope (Chumme) with to intense
579 snowmelt and by underestimation the small snow cover at Ried. In contrast, SM1 (blue line)
580 and SM2 (brown line) with standard meteorology cannot reproduce the observed snow
581 dynamics at any station.

582 Two conclusions can be drawn from this comparison: (1) the usage of the extended snowmelt
583 module SM2 (light green line, Figure 9) is necessary to reproduce the snowmelt, and (2) using
584 the adjusted meteorology and model (right panel, Figure 9) provides a better representation of
585 the snow cover depth and a higher amount of rainfall within the Milibach catchment.
586 However, none of the models are able to reproduce the observed discharge peak (maximum
587 flow is 9.3 m^3/s simulated vs. 32 m^3/s estimated). Only a strong reduction of the runoff
588 response times for direct-flow and interflow from this subcatchment (kd and ki, Table 2) leads
589 to a further concentration of discharge and a peak of 24.6 m^3/s (Figure 9, dotted orange line).
590 These two parameters are normally calibrated against an observed hydrograph, but as the

591 Milibach catchment is ungauged, the adjustment of the parameters is speculative but still
592 within a reasonable range.

593 Applying this adjusted model to the entire Lonza catchment provides also a good
594 representation of the flood peak at Blatten and Ferden (magenta line, Figure 7, right).
595 However, there are large overestimates in the diurnal melting cycles before the event due to
596 the overestimation of the SM2 melting rates. The adjusted model therefore is only valid for
597 the rain-on-snow flood. Still, the reliability of this model version for the time of the flood
598 peak is higher than of previous versions, as the observed catchment's internal characteristics,
599 such as precipitation distribution and snow depletion, are incorporated.

600 The retrospective modeling of the flood event demonstrated the importance of both latent and
601 sensible energy in the melting process, as suggested by the analysis of the local meteorology.
602 Moreover, the refinement of the meteorology was important for representing the strong
603 heterogeneous runoff pattern. Still, some limitations remain in the representation of the flood
604 peak of Milibach (25 m^3/s simulated vs. 32 m^3/s estimated); these limitations can be ascribed
605 to limitations in the representation of meteorological values, uncertain model parameters
606 and/or uncertainties in the observations. A further increase of local precipitation amounts
607 (+15%) in the Milibach catchment led to a flood peak of 31 m^3/s (not shown here), but
608 resulted in an overestimation at the gauge Lonza, Ferden, too.

609 Table 3 summarizes the water fluxes and the hydrological runoff coefficients for this event as
610 simulated using the SM2 model under standard meteorology and parameters and under
611 refined meteorology with adjusted parameters. For the two larger catchments, differences
612 between the versions are small, with little less snow and runoff applying the refined
613 meteorology. However, for the Milibach catchment, the changes are significant. The refined
614 meteorology shifts the proportions of solid and liquid precipitation, reducing the influence of
615 snowmelt and enhancing direct runoff from rainfall. As the snow cover was not entirely
616 melted and soils were filled up during the flood event, there even was the potential for an
617 even higher flood. Considering only rainfall as the input, the runoff coefficient Ψ was
618 calculated with $\Psi>1$, which emphasized the strong contributing role of snow for this event.
619 30% of the flood water originated from snow in each of the (sub-) catchments using the
620 optimal model configuration. Snowmelt contribution under standard meteorology and SM2
621 approach is remarkably high (at least 62%).

To conclude, using standard meteorology, the peak optimized hydrological model is able to approximately reproduce the flood peak at the catchment scale. But a detailed analysis at the subcatchment scale showed that these reproductions were due to the wrong reasons: Using uniformally distributed precipitation amounts in the catchment and a runoff promoting snow cover (SF = 0.9) resulted in a correct representation of the flood peak of the Lonza, but failed to reproduce the uneven distributed flooding in the tributary rivers and strongly underestimated the flood peak at the Milibach. The optimal hydrological model reproduced flood peaks at the catchment and subcatchment scale reasonable well only after the refinement of the meteorology and a more extensive adjustment of model parameters.

3.4 Predictability of the event

To evaluate the predictability of the event, we used the COSMO-2 forecast data 6, 12, and 18 hours in advance of the flood peak as the input data for the selected optimized model. Figure 11 displays rain and snow in the Loetschen valley and discharge at Lonza, Blatten and at Blatten, Ferden. The meteorology shown in Figure 11 was taken from the COSMO-2 output 12 hours before the flood peak occurred at 1200 UTC on 10 Oct. (rain: lightblue bars, snow: white bars; temperature curve in red) and compared with the refined meteorology (rain: blue bars, snow: yellow bars, temperature curve in black). COSMO-2 data (12h before flood peak) underestimate both the temperature increase and the precipitation amount in the morning of 10 Oct., resulting in a strong underestimation of the flood peak (25 m^3/s, 18 h in advance; 24.8 m^3/s 12 h in advance; and 35 m^3/s, 6 h in advance at Lonza, Blatten). The forecast 6 hours in advance resulted at least in a flood peak at the 2 year-return level (35 m^3/s). This corresponds to a medium hazard level at Lonza, Blatten. Comparing the total precipitation sums on 10 Oct. of the COSMO-2 forecast data (12h in advance, Lonza at Ferden catchment: 71.7 mm, Milibach catchment: 72 mm), standard meteorology (Lonza at Ferden catchment: 90.1 mm, Milibach catchment: 87.1 mm), and refined meteorology (Lonza at Ferden catchment: 112.8 mm, Milibach catchment: 164.7 mm), and regarding that using the standard meteorology, a higher flood peak was achieved (Figure 7, left panel), the underestimation of precipitation is not the only crucial deviation. Lower temperature increase in the night and morning of 10 Oct. led to a higher proportion of snowfall instead of rainfall on 10 Oct. and reduced snowmelt. In addition, it should be noted that using the optimized hydrological model and the best forecast data available (6 hours in advance), the predicted flood peak at Lonza, Ferden was still underestimated by at least 50%.

654

655 ## 4 Discussion

656 Extreme flood events typically result from adverse spatial and/or temporal combinations of
657 factors: Spatially, when intense weather occurs over particularly vulnerable regions (sealed,
658 saturated, steep); temporally, when a particular sequence of (not necessarily extreme) weather
659 conditions result in an extreme flood. In the present case, a temporally adverse sequence of
660 weather conditions can be traced back to the successive interaction of two (a cold and a
661 substantially warmer) air masses with the complex alpine topography. Compared to a
662 climatology of ERA-interim reanalysis October temperatures, the temperatures of the air
663 masses were anomalous but not extreme. The very rapid transition between the two air masses
664 was, however, highly unusual. The amount of moisture transported towards the Alps during
665 the rainfall event was exceptional. This moisture was transported over the Atlantic and around
666 the Azores high in a narrow corridor of moist air that fulfills the criteria to be called
667 "atmospheric river" (AR, see for ex. Bao et al., 2006, Ralph and Dettinger 2011).

668 While ARs are known to cause river flooding, especially on the west coast of northern
669 America (Ralph et al., 2006), little focus has been placed on the effects of ARs in Europe.
670 Knippertz and Wernli (2010) and Stohl et al. (2008) showed the presence of ARs in Europe,
671 but linking these wet air masses to floods has seldom been performed for that region.
672 Recently, Lavers and colleagues proved that major flood events in Great Britain (Lavers et al.,
673 2011) and annual maxima of precipitation in Western Europe (Lavers and Villarini, 2013) are
674 directly linked to AR. Stohl et al. (2008) were able to relate two flood events to ARs that were
675 formed by extratropical transitions of tropical cyclones.

676 This flood event is not only a result of the high precipitation amounts brought upon the Alps
677 by an AR; it is also a result of presence of fresh snow and of the intense temperature increase
678 that accompanied the moisture. The important role of the freezing level and snow-covered
679 area during rain-on-snow events was stressed by McCabe et al. (2007). Minimum and
680 maximum temperature levels must suit the elevation distribution of the affected snow-covered
681 valley to become problematic. Here, the 9 K temperature increase during the night of 9 Oct. to
682 10 Oct. activated the melting of the snow cover up to an elevation of 3,000 m a.s.l., which is
683 81 % (1,400 m a.s.l. to 3,000 m a.s.l.) of the valley area. The snow cover in the Loetschen
684 valley was hence very sensitive to this temperature increase, and accordingly, 30 % of the
685 total runoff water originated from snowmelt (Table 3).

686 In addition to this synoptic scale meteorological situation, the intensity of the rain-on-snow
687 event was highly variable at the valley scale. Evidence points to the important role of a cavity
688 circulation (upslope winds and formation of a surface cloud). This interpretation is consistent
689 with findings of several other studies where seeder-feeder effects are known to cause
690 significant local enhancements of the precipitations amounts (e.g., Roberts et al., 2009, Gray
691 and Seed, 2000). In Pennsylvania, Barros and Kuligowski (1998) found that "leeward-side
692 effects" enhance the local precipitation during rain-on-snow events and that there is a
693 correlation between "leeward-side effects" and strong hydrological flooding.

694 The cavity circulation not only enhanced the rainfall amount but also brought warm and moist
695 air masses in direct contact with the snow cover, resulting in intensified snowmelt through
696 sensible and latent heat transfer. Especially wind speed and humidity are essential for an
697 enhanced snowmelt as indicated by the melting equations: Assuming a relatively small
698 degree-day-factor of 0.5 for latent heat melting and only 1 m/s wind speed, 40 mm of rainfall
699 are necessary to generate the same amount of snowmelt from rainfall as from condensation.
700 This relation gets even more unbalance with higher wind speeds and degree-day-factors.
701 Strong surface winds, warm temperatures and high humidity indeed proved to contribute
702 directly to high snowmelt rates recorded in catastrophic rain-on-snow floods like in 1996 in
703 the Pacific Northwest (Marks et al., 1998) and in northern Pennsylvania (Leathers et al.,
704 1998). Our findings are consistent with these studies.

705 The application and the adjustment of the hydrological model for this flood reconstruction
706 confirmed the observed rapid response of the catchment to the rainfall and snowmelt. We
707 emphasize the importance of latent energy for the rapid snowmelt process because only the
708 snow module considering sensible *and* latent heat flow (SM2) was able to reproduce the snow
709 depletion. The importance of latent and sensible heat for snowmelt during rain-on-snow
710 events is consistent with results from other studies, e.g., (Marks et al., 1998), in which an
711 energy-balance model was applied to a rain-on-snow event.

712 Besides the strong energy input, snow cover structure is crucial in explaining the rapid runoff.
713 Kroczynski (2004) compared two similar rain-on-snow events with difference consequences,
714 one leading to a major flood and one without any flooding. He argued that the cause for the
715 major flood was the prior condition of the snow cover (a ripened snow cover) that led to a
716 saturated snow cover. In the present case, the snow cover was not ripe but rather fresh. But,
717 the snow cover up to 2,700 m a.s.l. was modeled to be saturated shortly after midnight on 10

718 Oct. by the lighter preceding rainfall, so the subsequent heavy rainfall (on the morning of 10
719 Oct.) fell on a saturated / ripe snow cover. This is although the water holding capacity was
720 increased from 10% to 20% - according to Jones et al. (1983) a reasonable value during
721 intense snowmelt periods. The WSL/SLF (Jonas et al. 2013) analyzed the role of the snow
722 cover for the flood event in detail using the 1D SNOWPACK model. Confirming our model
723 results, they concluded that the snow cover up to an elevation of 2,000 m a.s.l. in the
724 Loetschen valley was saturated when rain starts to fall. Furthermore, the modelled snowmelt
725 sum in this study agrees with results of a detailed snow model (Jonas et al. 2013) at the SLF
726 station Gandegg. This agreement also proves the validity of our snowmelt adjustment despite
727 uncertainties in the determination of the snow density. Singh et al. (1997) experimentally
728 showed that saturated snow cover produces a very rapid runoff response and maximum melt
729 flow. We conclude that the snow cover in the Loetschen valley was saturated before or shortly
730 after the rain started to fall, depending on elevation. This enabled a rapid direct runoff during
731 intensive rainfall and explains the short response time in the Milibach tributary catchment
732 where maximum precipitation occurred. Hence, the decrease of direct and interflow travel
733 time in the hydrological model was found essential to reproduce the flood peak.

734 However, there are also some limitations in our findings: Rapid snowmelt release from snow
735 cover is not reproduced in a physical manner in the hydrological model WaSiM-ETH, but
736 rather captured by adjusting these runoff response times. The adjustments of the runoff time
737 are uncertain as they are not validated with constantly measured discharge. WaSiM-ETH is
738 further limited as it uses a fixed water holding capacity in the snow and homogenous snow
739 structures. A coupling of WaSiM-ETH with a snow model might give a much better process
740 representation. Finally, missing runoff data at the gauge for the Lonza at Ferden (Figure 7)
741 make the determination of the flood peak uncertain. This is even more important as this gauge
742 covers 2/3 of the Loetschen valley and hence represents most of the flood causing processes.
743 However, due to the temporal agreement of the flood peak of different model versions and the
744 last data point measured at Ferden, we asssume that the flood peak was covered.

745 Comparing our findings with the cited studies, our interpretation about the major processes
746 and the model adjustments is confirmed. However, we were unable to simulate the estimated
747 runoff-peak of 32 m^3/s in the Milibach catchment. This might be partly due to an
748 underestimation of the measured rainfall, or it might be due to a further concentration of the
749 runoff. In addition, because the flood peak was estimated by field observations, the estimated

750 value itself is uncertain, even though it was performed by an expert (unpublished data,
751 Geoplan Naturgefahren). Despite the extensive observations available in the Loetschen valley
752 and even though we were able to reproduce the course of the event with a hydrological model,
753 the exact flood magnitude in the Milibach catchment and the response time of the catchment
754 remains uncertain due to uncertainties of observations and in the hydrological model.

755 Using the COSMO-2 forecast data as input to drive the optimized hydrological model, we
756 found that the flood peak was substantially underestimated; the forecasted peak flow was a
757 two year event (Lonza at Blatten gauge: 35 m^3/s). Comparing this underestimated flood peak
758 (60 m^3/s, Figure 11) from a "perfect" hydrological rain-on-snow model under forecasted
759 meteorology with the flood peak gained from the standard hydrological model under "perfect"
760 meteorology (75 m^3/s, Figure 7 right panel), it can be concluded that the slightly greater error
761 origins from the imperfect meteorological forecast data. We found a combination of
762 insufficient precipitation and a weaker temperature increase than observed (during the night
763 of 9 Oct. to 10 Oct.) that resulted in insufficient runoff. A reason for this underestimation
764 might be an unrealistic representation of meteorological processes by COSMO-2 at a small
765 scale like the Milibach catchment (3.3 km^2). The model performance of the COSMO-2
766 precipitation has been evaluated against coarser resolution models and radar based
767 observations by Weusthoff et al. (2010). They found that COSMO-2 to represent the
768 convective precipitation such as the precipitation in the present study much better than coarser
769 NWPs. Strikingly, the spatial pattern of the COSMO-2 precipitation (not shown here) was in
770 good agreement with our station measurements. However, the temperature increase and
771 precipitation amounts were not well predicted. This underlines findings by Jasper et al. (2002)
772 who emphasized the gross effect of small deviations in temperature and precipitation forecast
773 data on hydrological projections.

774 While the results of this case study are primarily limited to the catchment, the special
775 meteorological situation causing the flood, and the hydrological model applied, the question
776 arises which findings can be transferred to other areas. Viviroli et al. (2009) showed that
777 model parameters can be regionalized even for flood calibrations. However, it remains
778 unclear whether this regionalization procedure holds also true for model settings representing
779 rain-on-snow events. But Hermi et al. (2013) reanalyzed the same flood event in different
780 Swiss catchments with the hydrological model PREVAH and confirmed our finding that the
781 uncorrected standard model was not able to adequately reproduce the flood event and that

runoff response times as well as snowmelt parameters need to be adjusted to fit the model against observations. It can be argued that these parameters and configurations have to be adjusted in general for the presentation of rain-on-snow events, independent from the catchment, the meteorological conditions, and hydrological model used. Thus, the direct transferation of model parameters and configurations is uncertain, but the information which parameters need to be adjusted remains valid.

This study showed that the combined analysis using meteorological and hydrological methods and knowledge can highly improve the understanding of an event. A detailed understanding anables the process-proximity of the hydrological modelling and highlights the key model parameter and configurations, namely the adjustment of the runoff response times and the use of a more sophisticated snowmelt model that uses latent and sensible heat.

Furthermore, we found that is it not possible to adequately reproduce the rain-on-sow event with basic model configuration. This finding has some implication for the hydrological now-/forecasting, as it calls for an addition forecast using rain-on-snow adjusted models. This might be either done using multi-model approaches (e.g. Ajami et al. 2006, WMO 2011) or by applying an alternative prediction scenario when rain-on-snow events are likely to occur.

Conclusion

The goal of this study was to reconstruct the hydro-meteorological anatomy of a rain-on-snow flood event, find the triggering processes, and estimate the predictability of the event. Firstly, we were able to trace the meteorological causes and the relevant hydrological process behind this event. Important atmospheric ingredients of the flood event were: (a) a combination of exceptional amounts of moisture impacting upon orography when an atmospheric river reached Switzerland after a cold period with significant snowfall, (b) potentially local rainfall enhancement by a cavity circulation, and (c) enhanced snowmelt due to additional latent heat input from the warm and moist air. Overall, this study contributes to the understanding of other flood events that were triggered by ARs in Europe by adding another process region (Switzerland) and another process type (rain-on-snow event). Furthermore, we confirm previous studies on the importance of leeward circulation as well as latent and sensible heat fluxes during rain-on-snow flood events.

Secondly, thanks to very high spatial resolution of the meteorological measurements in the Loetschen valley, we are able to investigate variations in the precipitation pattern at the valley scale. This allows us to reconstruct the flood peak at the subcatchment scale. The transfer of latent heat provided by precipitation and condensation, the rapid saturation of the snow cover and subsequent fast runoff, and the activation of snowmelt in a large part of the catchment were crucial processes. Extensive observations and model calibration at this particular catchment were necessary to provide enough information to adjust a standard hydrological model to this rain-on-snow flood.

Thirdly, despite the effort made to understand this flood event and to adjust the hydrological model, the ability of the hydro-meteorological model chain to forecast such a rain-on-snow flood is still limited by the quality of the numerical weather predictions, especially in terms of precipitation and temperature. Interestingly, the errors due to hydrological model and to the meteorological forecasts were slightly of the same magnitude with the meteorological forecasts being more important; the underestimation of the discharge being of about 50% due to the forecast data and 37.5 % due to hydrological model parameterization. In addition, only with a dense network of “private” meteorological stations – despite all uncertainties due to unheated instruments – was it possible to reconstruct the local meteorological conditions that caused the flood. This stresses the need to maintain and extend the network of meteorological, snow and discharge gauging stations to improve and extent our observations and hence to

improve future predictions. The good news is that while recent hydrological models need to be adjusted, they are capable of reacting sensitively to rain-on-snow events. Further studies on hydrological modeling of rain-on-snow events will be necessary to demonstrate the transferability of these adjustments to other events or regions.

The flood event on the 10th of October in the Loetschen valley was a vast rain-on-snow event, caused by a temporally adverse sequence of otherwise not extreme processes (apart from the amount of atmospheric moisture transport). The flood can be reconstructed and predicted if the hydrological model is adjusted to react sensitively to these events and if the meteorological forecasts of precipitation and temperature are sufficiently accurate.

In a more general perspective, this study showed that rain-on-snow events cannot be simulated with a standard model set up, but need a special model configuration. Hence, operational forecast my need to run an adjusted model when rain-on-snow events are likely to happen.

Acknowledgement

We would like to thank Jules Sailer from Geoplan Naturgefahren, Steg, for fruitful discussions and detailed information about the event. Special thanks also to Nico Piaget (ETH Zurich) for helpful discussion and information about the meteorological development of the event. In addition, we acknowledge the kind provision of data by EnAlpin (gauge Ferden), MeteoMedia (meteorological station Wiler), SLF (meteorological and IMIS station Gandegg and Sackhorn), MeteoSwiss (official meteorological station data, gridded precipitation), and BAFU (discharge from Lonza, Blatten). We acknowledge an anonymous reviewer and Dr. Stephan Pohl for very constructive comments that helped to improve the manuscript.

References

Ajami, N., Duan, Q, Gao, X, Sorooshian, S.: Multimodel Combination Techniques for Analysis of Hydrological Simulations: Application to Distributed Model Intercomparison Project Results. Journal of Hydrometeorology, 7, 755-768, 2006.

Anderson, E. A. (Ed.): National Weather Service river forecast system: snow accumulation and ablation model, National Oceanographic and Atmospheric Administration (NOAA) Technical Memorandum NWS-HYDRO, 17, U.S. Department of Commerce, Silver Spring, MD., 238 pp., 1973.

Andres, N., Badoux, A., Hilker, N., and Hegg, C.: Unwetterschäden in der Schweiz im Jahre 2011, Wasser, Energie, Luft, 104, 41–49, 2011.

Bao, J. W., Michelson, S., Neiman, P., Ralph, F. M., and Wilczak, J.: Interpretation of Enhanced Integrated Water Vapor Bands Associated with Extratropical Cyclones: Their Formation and Connection to Tropical Moisture, Mon. Wea. Rev., 134, 1063–1080, doi:10.1175/MWR3123.1, 2006.

Barros, A. P. and Kuligowski, R. J.: Orographic Effects during a Severe Wintertime Rainstorm in the Appalachian Mountains, Mon. Wea. Rev., 126, 2648–2672, 1998.

Beven, K.: Rainfall-runoff modelling: The primer, Wiley, Chichester, 2001.

Börst, U.: Nachhaltige Entwicklung im Hochgebirge.: Eine Systemanalyse von Mensch-Umwelt-Szenarien im Lötschental (Zentral-Alpen)., Dissertation, Bonn, 214 pp., 2005.

Bundesamt für Umwelt (Ed.): Ereignisanalyse Hochwasser August 2007, Bern, 209 pp., 2009.

Cloke, H. and Pappenberger, F.: Ensemble flood forecasting: A review, Journal of Hydrology, 375, 613–626, doi:10.1016/j.jhydrol.2009.06.005, 2009.

Conway, H. Storm Lewis: A rain-on-snow event on the Milford Road, New Zealand. International Snow Science Workshops (ISSW) Proceedings of Professional Papers and Poster Talks, 557-564, http://arc.lib.montana.edu/snow-science/item.php?id=1137, last access: 21.10.2013, 2004.

Dee, D. P., Uppala, S. M., Simmons, A. J., Berrisford, P., Poli, P., Kobayashi, S., Andrae, U., Balmaseda, M. A., Balsamo, G., Bauer, P., Bechtold, P., Beljaars, A. C. M., van de Berg, L., Bidlot, J., Bormann, N., Delsol, C., Dragani, R., Fuentes, M., Geer, A. J., Haimberger, L.,

Healy, S. B., Hersbach, H., Hólm, E. V., Isaksen, L., Kållberg, P., Köhler, M., Matricardi, M., McNally, A. P., Monge-Sanz, B. M., Morcrette, J.-J., Park, B.-K., Peubey, C., Rosnay, P. de, Tavolato, C., Thépaut, J.-N., and Vitart, F.: The ERA-Interim reanalysis: configuration and performance of the data assimilation system, Q.J.R. Meteorol. Soc., 137, 553–597, doi:10.1002/qj.828, 2011.

Gray, W. R. and Seed, A. W.: The characterisation of orographic rainfall, Meteorol. Appl., 7, 105–119, 2000.

Green, W. and Ampt, G.: Studies of soil physics, part I - the flow of air and water through soils, Journal of Agricultural Science, 1–24, 1911.

Hermi, S., Hofer, M., Zappa, M.: Hydrometeorologische Analyse des Hochwasserereignisses vom 10. Oktober 2011. Eidgenössische Forschungsanstalt WSL, http://www.wsl.ch/fe/gebirgshydrologie/wildbaeche/projekte/unwetter2011/HW2011_Fachbericht_Hydrologie_WSL.pdf, last access 08.01.2014, 2013.

Hölzel, H., Rössler, O., Diekkrüger, B.: Grope in the Dark – Hydrological modelling of the artificial Chicken Creek catchment without validation possibilities. Phyics and Chemnistry of the Earth, 36, 113-122, 2011.

Houze, R. A. and Medina, S.: Turbulence as a Mechanism for Orographic Precipitation Enhancement, J. Atmos. Sci., 62, 3599–3623, 2005.

Jasper, K., Gurtz, J., and Lang, H.: Advanced flood forecasting in Alpine watersheds by coupling meteorological observations and forecasts with a distributed hydrological model, Journal of Hydrology, 40–52, 2002.

Jonas, T.: Hydrometeorologische Analyse des Hochwasserereignisses vom 10.-11. Oktober 2011. Fachbericht Schneehydrologie. SLF. http://www.wsl.ch/fe/gebirgshydrologie/wildbaeche/projekte/unwetter2011/HW2011_Fachbericht_Schneehydrologie_SLF.pdf, last access 08.01.2014., 2013.

Jones, E., Rango, A., and Howell, S.: Snowpack liquid water determinations using freezing calorimetry, Nordic Hydrology, 14, 113–126, 1983.

Judson, A. and Doesken, A.: Density of freshly fallen snow in the central Rocky Mountains. , Bull. Amer. Meteor. Soc., 81, 1577-1587, 2000.

912 Kirchhofer, W. and Sevruk, B.: Mittlere jährliche korrigierte Niederschlagshöhen 1951-1980:
913 Kartenblatt 2.2, in: Hydrologischer Atlas der Schweiz, BAFU (Ed.), Bern, 2010.

914 Knippertz, P. and Wernli, H.: A Lagrangian Climatology of Tropical Moisture Exports to the
915 Northern Hemispheric Extratropics, J. Climate, 23, 987–1003, doi:10.1175/2009JCLI3333.1,
916 2010.

917 Kroczynski, S.: A Comparison Of Two Rain-On-Snow Events And The Subsequent
918 Hydrologic Responses In Three Small River Basins In Central Pennsylvania, Eastern Region
919 Technical Attachment, 4, 1–21, 2004.

920 Lavers, D. A., Allan, R. P., Wood, E. F., Villarini, G., Brayshaw, D. J., and Wade, A. J.:
921 Winter floods in Britain are connected to atmospheric rivers, Geophys. Res. Lett., 38,
922 L23803, doi:10.1029/2011GL049783, 2011.

923 Lavers, D. A. and Villarini, G.: The nexus between atmospheric rivers and extreme
924 precipitation across Europe, Geophys. Res. Lett., 40, 3259–3264, doi:10.1002/grl.50636,
925 2013.

926 Leathers, D. J., Kluck, D. R., and Kroczynski, S.: The Severe Flooding Event of January 1996
927 across North-Central Pennsylvania, Bull. Amer. Meteor. Soc., 79, 785–797, 1998.

928 Marks, D., Kimball, J., Tingey, D., and Link, T.: The sensitivity of snowmelt processes to
929 climate conditions and forest cover during rain-on-snow: a case study of the 1996 Pacific
930 Northwest flood, Hydrol. Process., 12, 1569–1587, 1998.

931 McCabe, G. J., Hay, L. E., and Clark, M. P.: Rain-on-Snow Events in the Western United
932 States, Bull. Amer. Meteor. Soc., 88, 319–328, doi:10.1175/BAMS-88-3-319, 2007.

933 Merz, R. and Blöschl, G.: A process typology of regional floods, Water Resour. Res., 39,
934 1340, doi:10.1029/2002WR001952, 2003.

935 MeteoSchweiz, Model Properties: Dynamics and Numerics, Physics, Data Assimilation, and
936 more.: http://www.meteoschweiz.admin.ch/web/en/research/consortia/cosmo/more_about/-
937 cosmo-2.html, last access: 18 January 2014, 2010

938 Pomeroy, J. W., Gray, D. M., Shook, K. R., Toth, B., Essery, R. L. H., Pietroniro, A.,
939 Hedstrom, N.: An evaluation of snow accumulation and ablation processes for land surface
940 modelling. Hydrol. Process., 12, 2339–2367, 1998.

941 Ralph, F. M., Neiman, P. J., Wick, G. A., Gutman, S. I., Dettinger, M. D., Cayan, D. R., and
942 White, A. B.: Flooding on California's Russian River: Role of atmospheric rivers, Geophys.
943 Res. Lett., 33, L13801, doi:10.1029/2006GL026689, 2006.

944 Ralph, F. M., and Dettinger, M. D.: Storms, floods, and the science of atmospheric rivers.
945 Eos, Transactions American Geophysical Union, 92(32), 265-266, 2011

946 Reinecke, P. A. and Durran, D. R.: Estimating Topographic Blocking Using a Froude Number
947 When the Static Stability Is Nonuniform, J. Atmos. Sci., 65, 1035–1048,
948 doi:10.1175/2007JAS2100.1, 2008.

949 Roberts, N. M., Cole, S. J., Forbes, R. M., Moore, R. J., and Boswell, D.: Use of high-
950 resolution NWP rainfall and river flow forecasts for advance warning of the Carlisle flood,
951 north-west England, Met. Apps, 16, 23–34, doi:10.1002/met.94, 2009.

952 Rössler, O., Diekkrüger, B., and Löffler, J.: Potential drought stress in a Swiss mountain
953 catchment-Ensemble forecasting of high mountain soil moisture reveals a drastic decrease,
954 despite major uncertainties, Water Resour. Res., 48, W04521, doi:10.1029/2011WR011188,
955 2012.

956 Rössler, O., Froidevaux, P., Börst, U., Rickli, R., Martius, O., and Weingartner, R.:
957 Ereignisanalyse Extremhochwasser Lötschental, Wallis, 10. Oktober 2011, Publikation
958 Gewässerkunde 553, GIUB, Bern, 2013.

959 Rössler, O. and Löffler, J.: Potentials and limitations of modelling spatio-temporal patterns of
960 soil moisture in a high mountain catchment using WaSiM-ETH, Hydrol. Process., 24, 2182–
961 2196, doi:10.1002/hyp.7663, 2010.

962 Schlemmer, L., Martius, O., Sprenger, M., Schwierz, C., and Twitchett, A.: Disentangling the
963 Forcing Mechanisms of a Heavy Precipitation Event along the Alpine South Side Using
964 Potential Vorticity Inversion, Mon. Wea. Rev., 138, 2336–2353,
965 doi:10.1175/2009MWR3202.1, 2010.

966 Schulla, J.: Model Description WaSiM: www.wasim.ch: http://www.wasim.ch/, last access:
967 30 July 2013, 2013

968 Singh, P., Spitzbart, G., Hübl, H., and Weinmeister, H.: Hydrological response of snowpack
969 under rain-on-snow events: a field study, Journal of Hydrology, 202, 1–20, 1997.

970 Stohl, A., Forster, C., and Sodemann, H.: Remote sources of water vapor forming
971 precipitation on the Norwegian west coast at 60°N–a tale of hurricanes and an atmospheric
972 river, J. Geophys. Res., 113, D05102, doi:10.1029/2007JD009006, 2008.

973 Sui, J., Koehler, G. Rain-on-snow induced flood events in southern Germany. Journal of
974 Hydrology, 252, 205-220, 2001.

975 Viviroli, D, Mittelbach, H., Gurtz, J., Weingartner, R.: Continuous simulation for flood
976 estimation in ungauged mesoscale catchments of Switzerland – Part II: Parameter
977 regionalisation and flood estimation results. Journal of hydrology, 377, 208-225, 2009.

978 Verbunt, M., Gurtz, J., Jasper, K., Lang, H., Warmerdam, P., and Zappa, M.: The
979 hydrological role of snow and glaciers in alpine river basins and their distributed modeling,
980 Journal of Hydrology, 282, 36–55, doi:10.1016/S0022-1694(03)00251-8, 2003.

981 Whitaker, A. C. and Sugiyama, H.: Seasonal snowpack dynamics and runoff in a cool
982 temperate forest: lysimeter experiment in Niigata, Japan. Hydrol. Process., 19, 4179-4200,
983 2005.

984 Weusthoff, T., Ament, F., Arpagaus, M., and Rotach, M. W.: Assessing the Benefits of
985 Convection-Permitting Models by Neighborhood Verification: Examples from MAP D-
986 PHASE, Mon. Wea. Rev., 138, 3418–3433, doi:10.1175/2010MWR3380.1, 2010.

987 Wirth, V., Kristen, M., Leschner, M., Reuder, J., and Schween, J. H.: Banner clouds observed
988 at Mount Zugspitze, Atmos. Chem. Phys., 12, 3611–3625, doi:10.5194/acp-12-3611-2012,
989 2012.

990 World Meteorological Organization: Manual on flood forecasting and warning, no. 1072,
991 World Meteorological Organization, Geneva, xii, [121], 2011.
992

Table 1: Meteorological stations in the catchment with the parameters measured, the elevation of the location, and the supporting institution.

ID cp. Figure 1	Meteorological Station	Institution	Elevation, m a.s.l.	Temperature	Precipitation	Snow height	Wind speed	Wind direction	Relative humidity
1	Ried	GIUB	1470	x	x	x	x	x	x
2	Chumme	GIUB	2210	x	x	x	x	x	x
3	Grund	GIUB	1855	x	x	x	x	x	x
4	Grossi Tola	GIUB	2880	x	x	-	x	x	x
5	Mannlich	GIUB	2250	x	x	x	x	x	x
6	Sackhorn	SLF	3200	x	-	-	x	x	x
7	Gandegg	SLF	2717	x	x	x	x	x	x
8	Wiler	Meteomedia	1415	x	x	-	x	x	x

Table 2: Summary of the most important parameter and how they were adjusted in the different model versions.

Model version	T0	C0	C1	C2	Kd Ferden/Blatten/Milibach	Ki Ferden/Blatten/Milibach	SF Ferden/Blatten/Milibach
standard	0	4	-	-	12 /12/12	24 /24/24	0.1 / 0.1 / 0.1
peak optimized	0	4	-	-	12 /12/12	24 /24/24	0.9 / 0.9 / 0.9
SM2	0	-	2.5	2.5	12 /12/12	24 /24/24	0.1 / 0.1 / 0.1
SM2, adjusted	0	-	3	3	12 /12/1	24 /24/1	0.1 / 0.1 / 0.1

1004 Table 3: Water fluxes, storages and characteristic values during the peak flow from 6 Oct.to
1005 10 Oct. 2011 for SM2 melt modules under standard and refined meteorology and parameters.

	Ferden (140 km^2)		**Blatten (78 km^2)**		**Milibach (3.3 km^2)**	
	Standard meteorology	refined meteorology	Standard meteorology	refined meteorology	Standard meteorology	refined meteorology
rain [mm]	93.6	94.5	75.5	77.4	92.6	167.9
snow [mm]	124.2	104.3	122.6	121.8	103.9	84.4
total runoff [mm]	102.2	95.7	92	80.3	109.3	188.4
direct flow [mm]	39.7	39.6	36.5	31.2	45.8	99.4
interflow [mm]	92.5	55.9	55.4	48.9	63.5	88.8
base flow [mm]	0	0.2	0	0.2	0	0.1
max. snow cover [mm]	85.3	62.3	102.9	79.6	97.3	72.1
snow cover after event [mm]	21.8	34.9	43.7	67.8	22.9	12.8
change in snow cover [mm]	-63.5	-27.4	-.59.2	-11.8	-74.4	-59.3
change in soil moisture [mm]	6.7	33.2	6.3	29.4	7.1	46.9
rainfall-runoff-coefficient [1/1]	1.09	1	1.22	1	1.18	1.1
snowmelt-runoff-ratio[1/1], Jasper et al. (2002)	0.62	0.3	0.64	0.1	0.68	0.3

1006
1007
1008
1009
1010

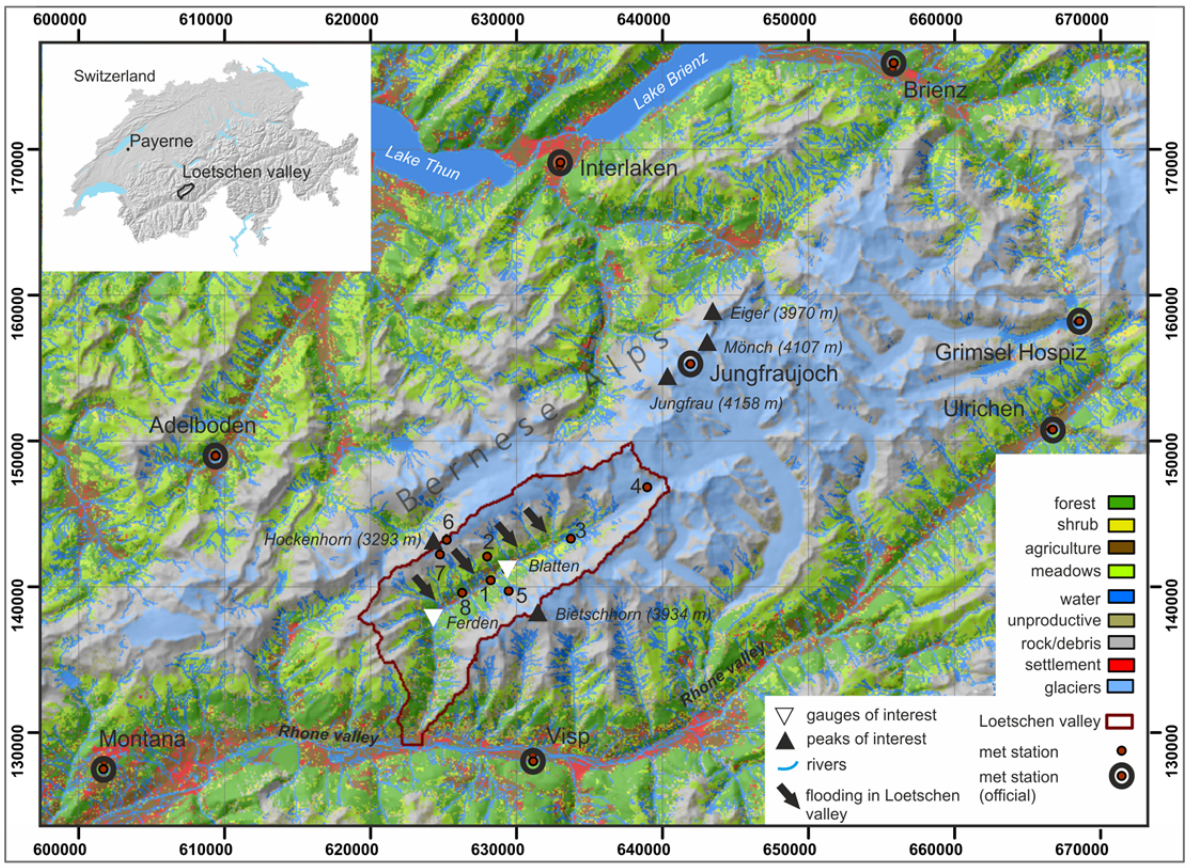

Figure 1: Location of the Loetschen valley in Switzerland and the land cover characteristics of the valley. The black arrows indicate the flooding rivers, red dots and black circles represent meteorological stations and white triangles represent discharge gauges. Recordings from the meteorological stations in the Loetschen valley will be analysed in section 3.2. The stations names are (1) Ried, (2) Chumme, (3) Grund, (4) Grossi Tola, (5) Mannlich, (6) Sackhorn, (7) Gandegg and (8) Wiler.

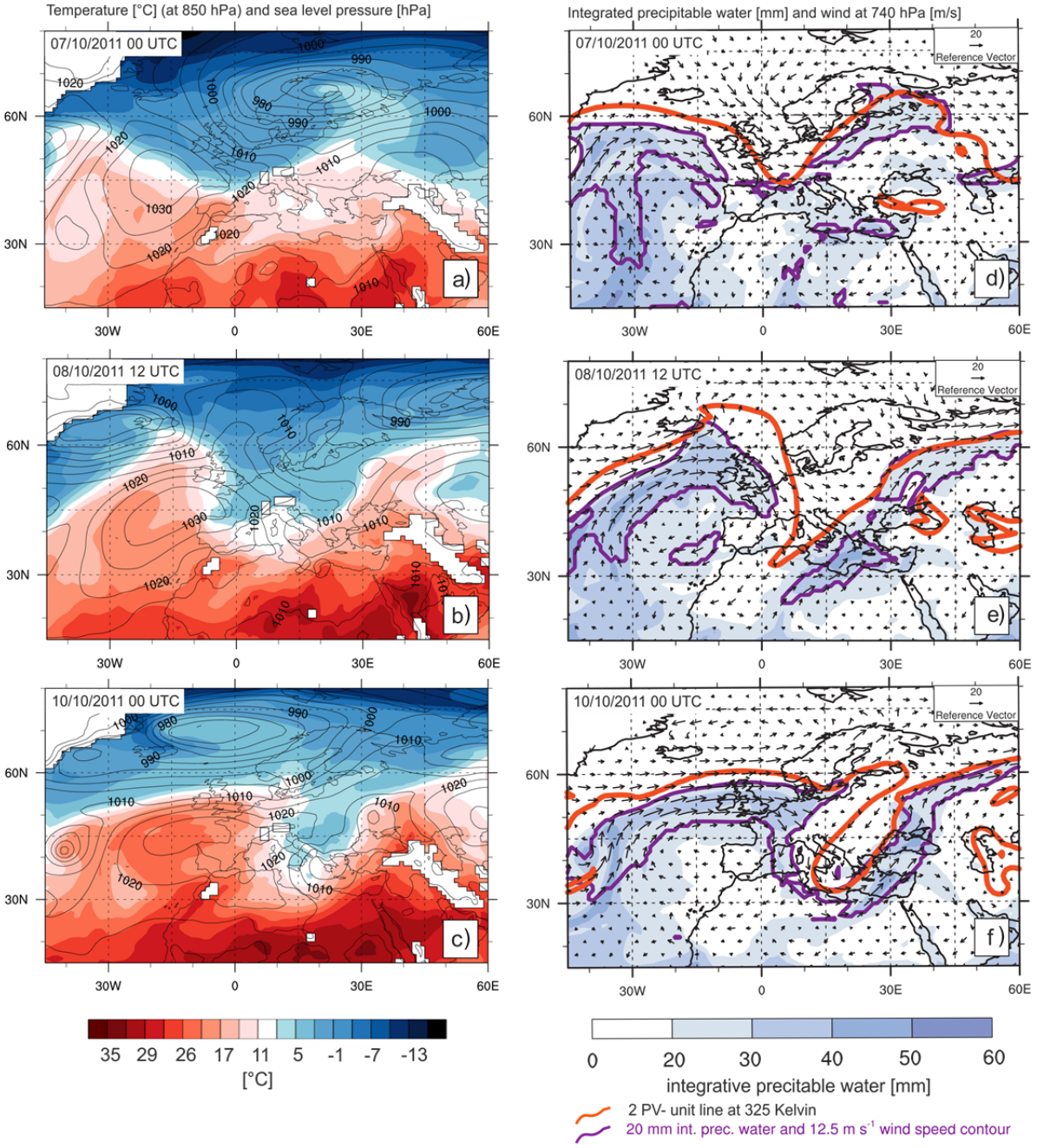

1021

1022 Figure 2: ECMWF reanalysis data at 7 Oct. 2011 00 UTC (top row), 8 Oct. 2011 12 UTC
1023 (middle row) and 10 Oct. 2011 00 UTC (bottom row). The left column (a-c) displays
1024 temperature in °C at 850 hPa (color) together with sea level pressure in hPa (contours). The
1025 right column (d-f) shows the vertically integrated precipitable water of the atmosphere in mm
1026 (color) together with the 740 hPa wind in m/s (arrows). The red line in these panels refers to
1027 the potential vorticity (PV) and illustrates the 2 PV unit limit on the 320 K isentrope. Violet
1028 lines in d-f indicate the outline of atmospheric river conditions, based on the definition by
1029 Ralph and Dettinger (2011).

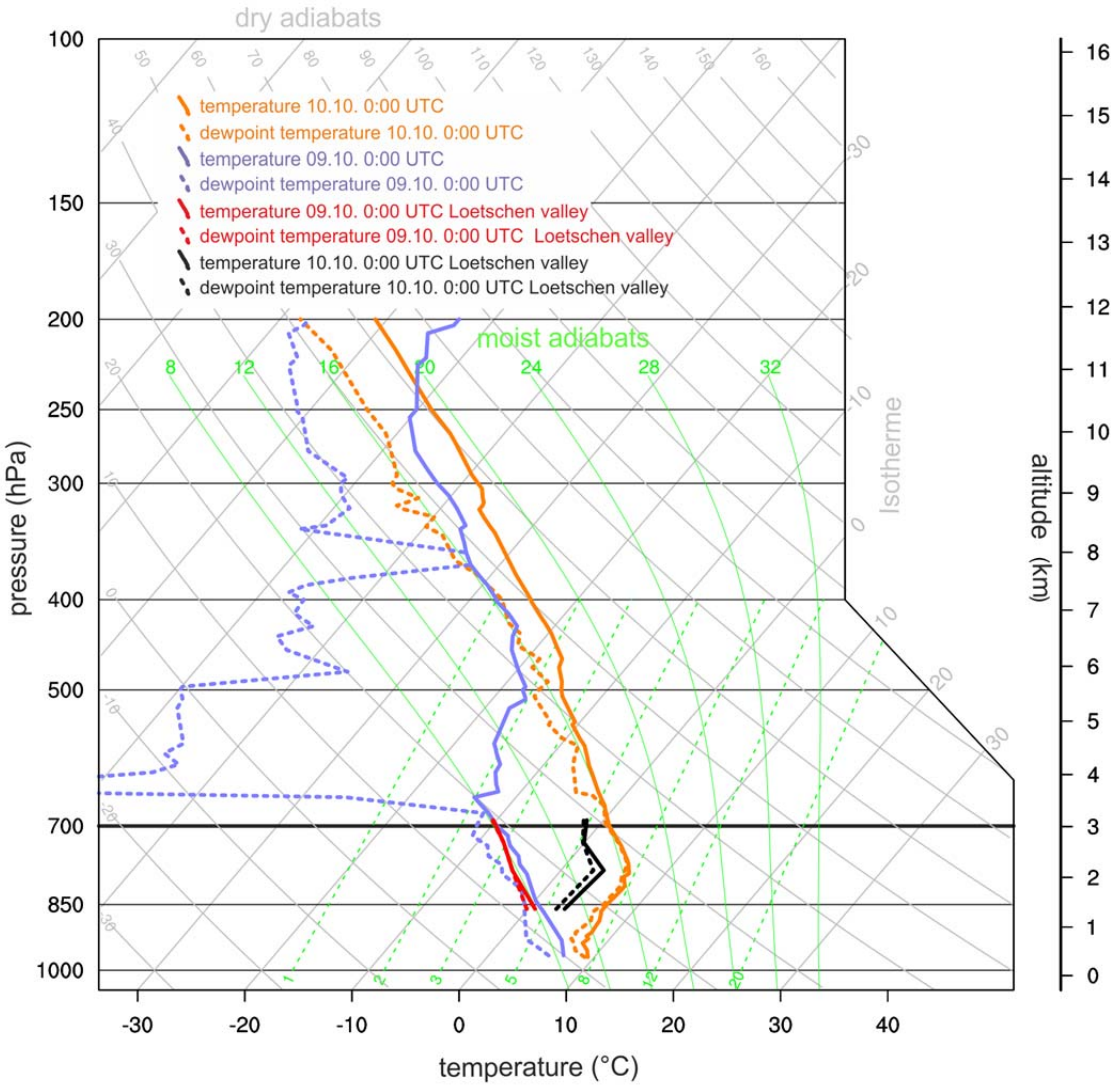

Figure 3: Skew-t-log-P-diagram showing the vertical atmospheric structure as measured from weather balloons launched at Payerne (cf. Figure 1) on 9 Oct. 2011 00 UTC (blue lines) and 10 Oct. 2011 00 UTC (orange lines). The profile of the Loetschen valley as retrieved by surface meteorological stations is included for comparison (red for 9 Oct. 00 UTC and black for 10 Oct. 00 UTC). The main ridge of the Loetschen valley has a mean elevation of approximately 3,000 m a.s.l. (thick line).

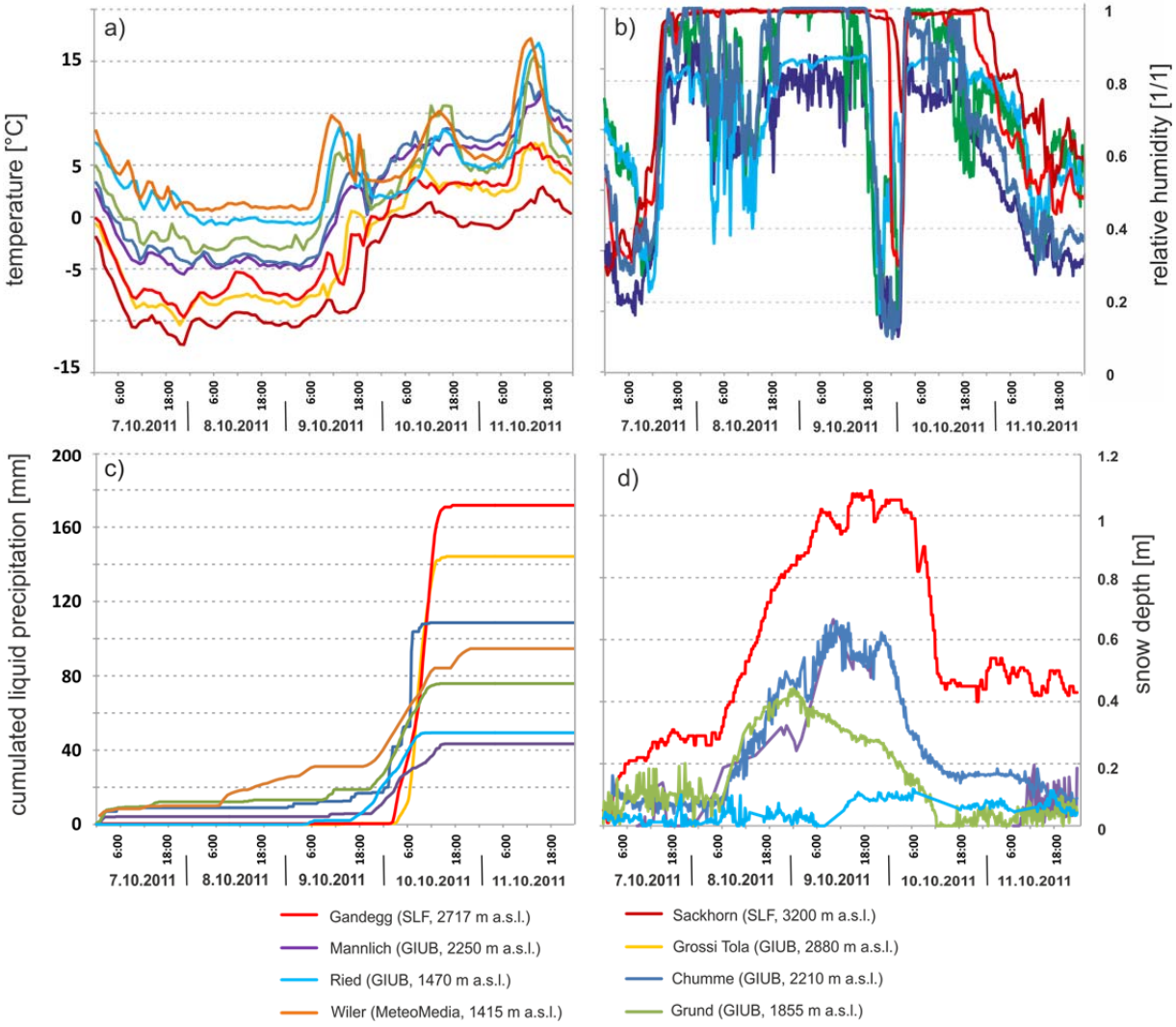

Figure 4: Temperature (a), relatively humidity (b), accumulated liquid precipitation (c), and snow height (d) measured at eight meteorological stations in the Loetschen valley. The time series describe the overall course of the weather and reveal strongly heterogeneous rainfall amounts.

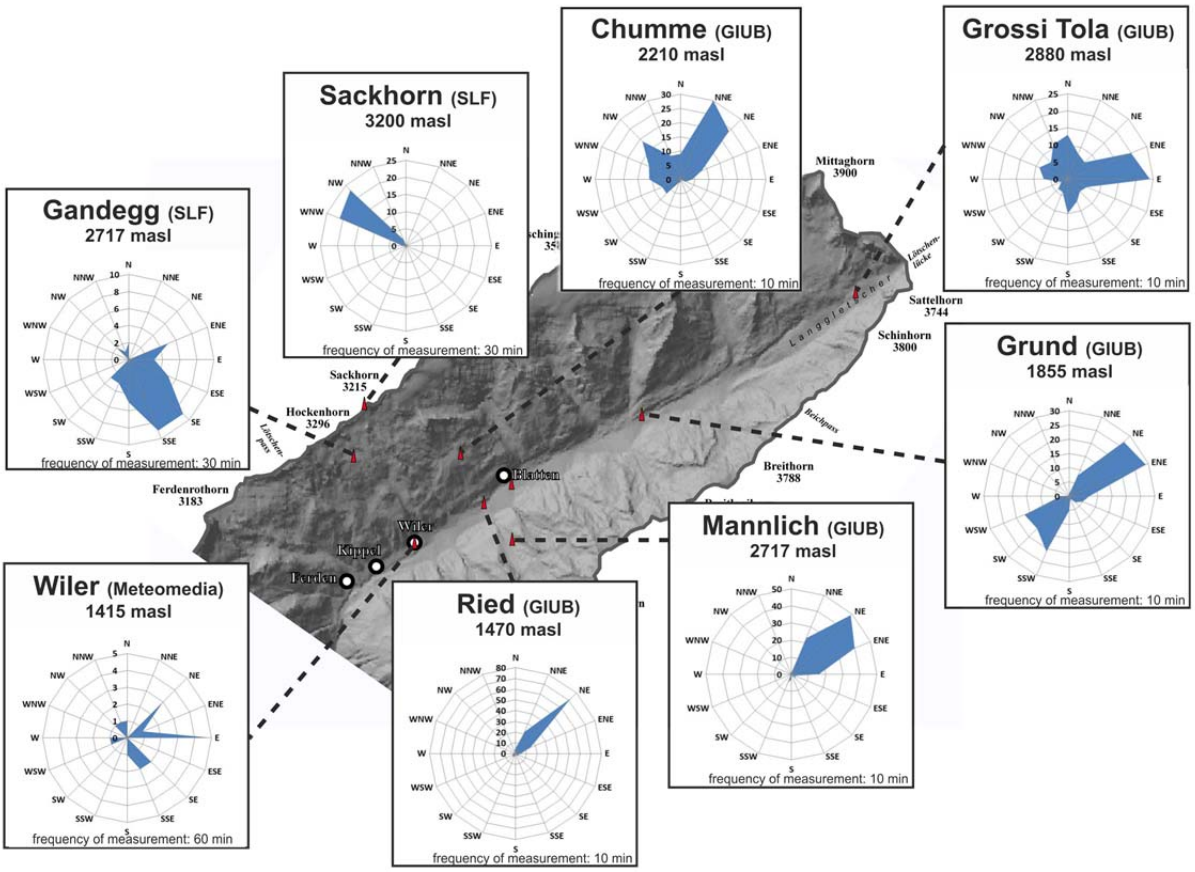

Figure 5: Frequency of two-meter wind directions from station measurements on 10 Oct in the Loetschen valley. The radial component of each direction (in blue) indicates the number of measurements when the wind was blowing from that respective direction in 24 hours. Note that the total number of measurements varies since wind is measured every 60, 30 or 10 minutes depending on the station. Particularly remarkable is that the neighbouring stations Sackhorn and Gandegg recorded opposite wind directions. This can be explained by the presence of a cavity circulation (schematized in fig. 6).

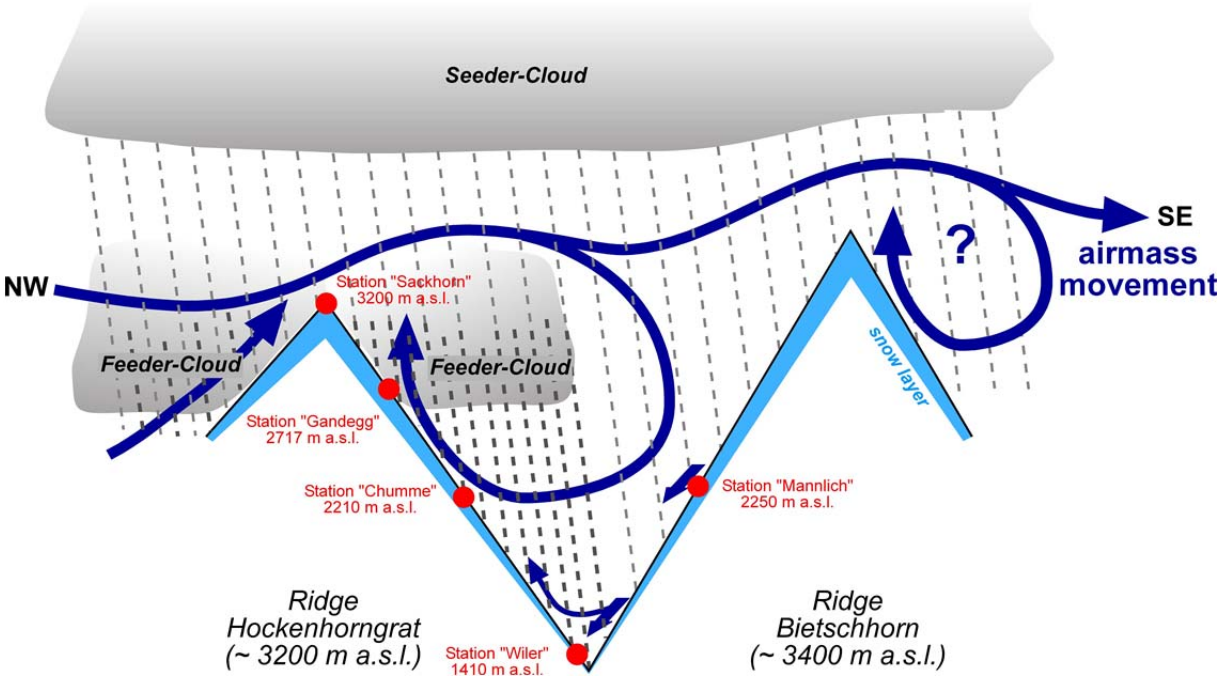

Figure 6: Schematic depiction of our interpretation of the atmospheric conditions. The question mark indicates that a second cavity circulation might be present in the adjacent valley, but we have no evidence.

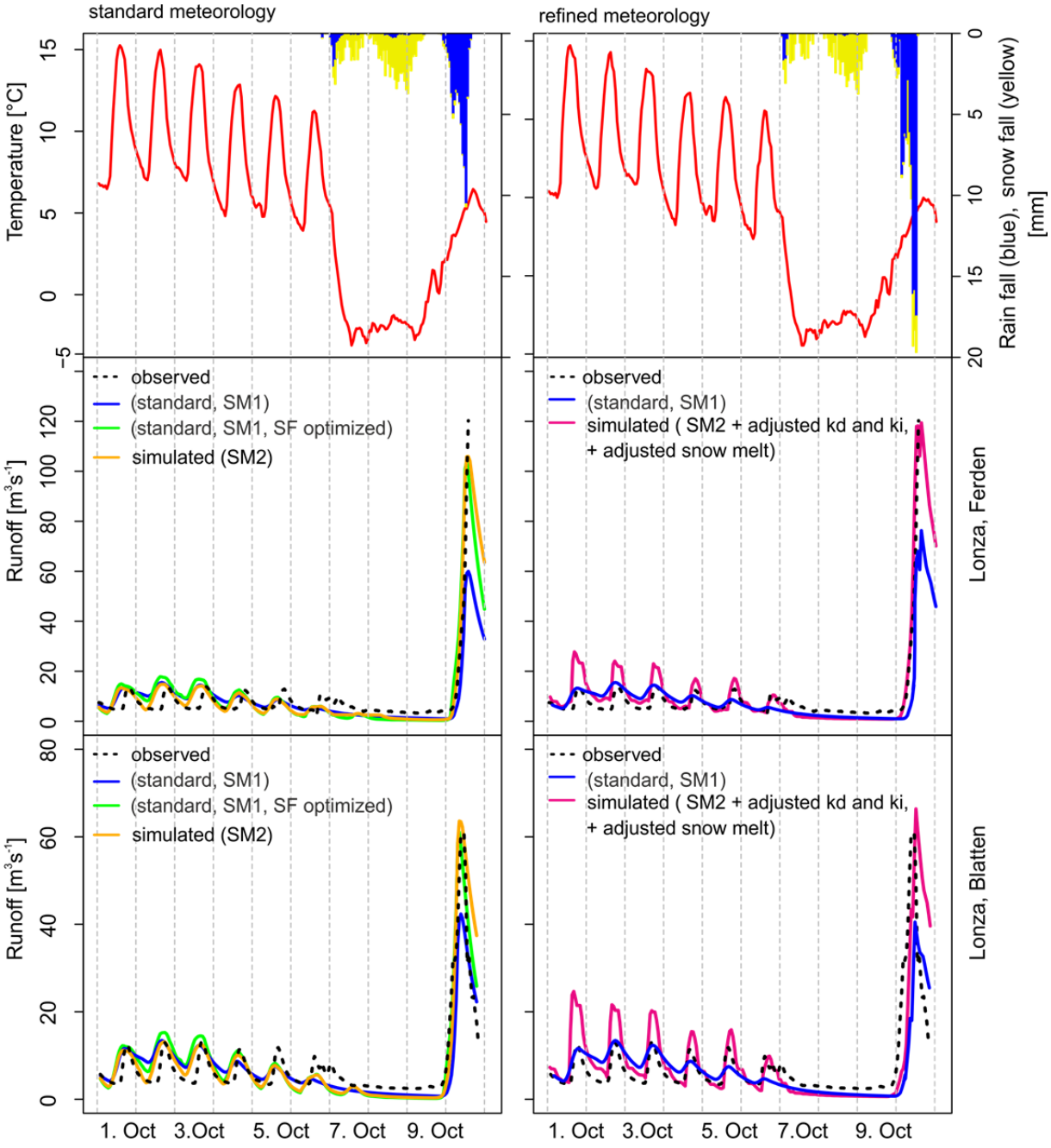

Figure 7: Retrospective modeling of the flood event at two gauges, Lonza, Ferden and Lonza, Blatten, under standard (left panel) and refined meteorology (right panel) shows that the standard WaSiM-ETH model set up (blue lines) is not able to replicate the observations (black dotted lines), while the three peak-optimized model set ups (orange, green, magenta lines) are capable of matching the observations. Meteorology is depicted as temperature (red line) and rainfall (blue) and snowfall (yellow) in the top row.

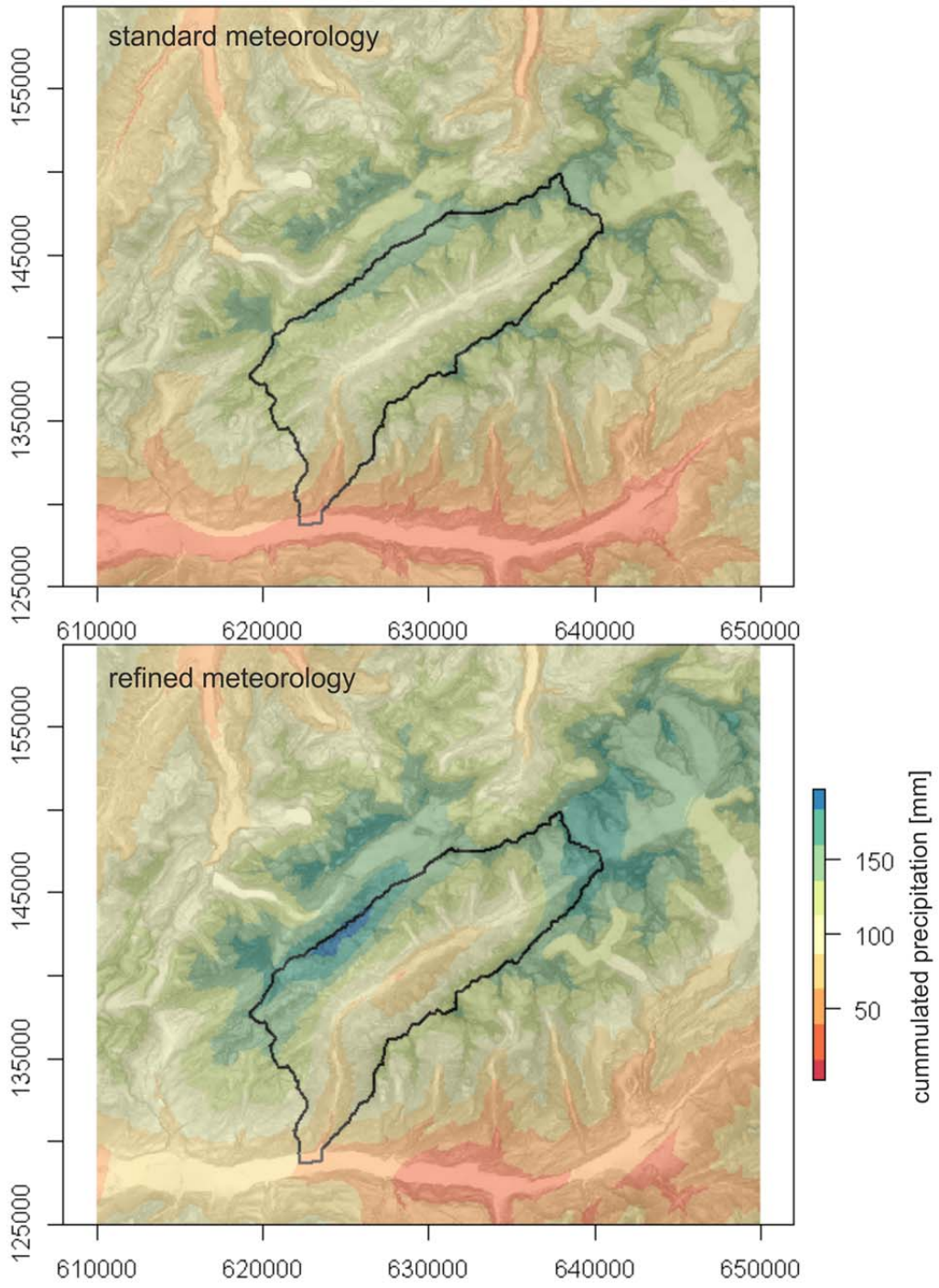

Figure 8 Accumulated liquid precipitation from 9 Oct. 14 UTC to 10 Oct. 20 UTC, as regionalized by the hydrological model using to the inverse distant and height regression approaches with the official meteorological stations and the SLF Gandegg station (cp. Figure 1), upper panel, and using the refined meteorology with all available meteorological stations with a correction function (lower panel) and a fixed southwest-northeast interpolation orientation following the topography.

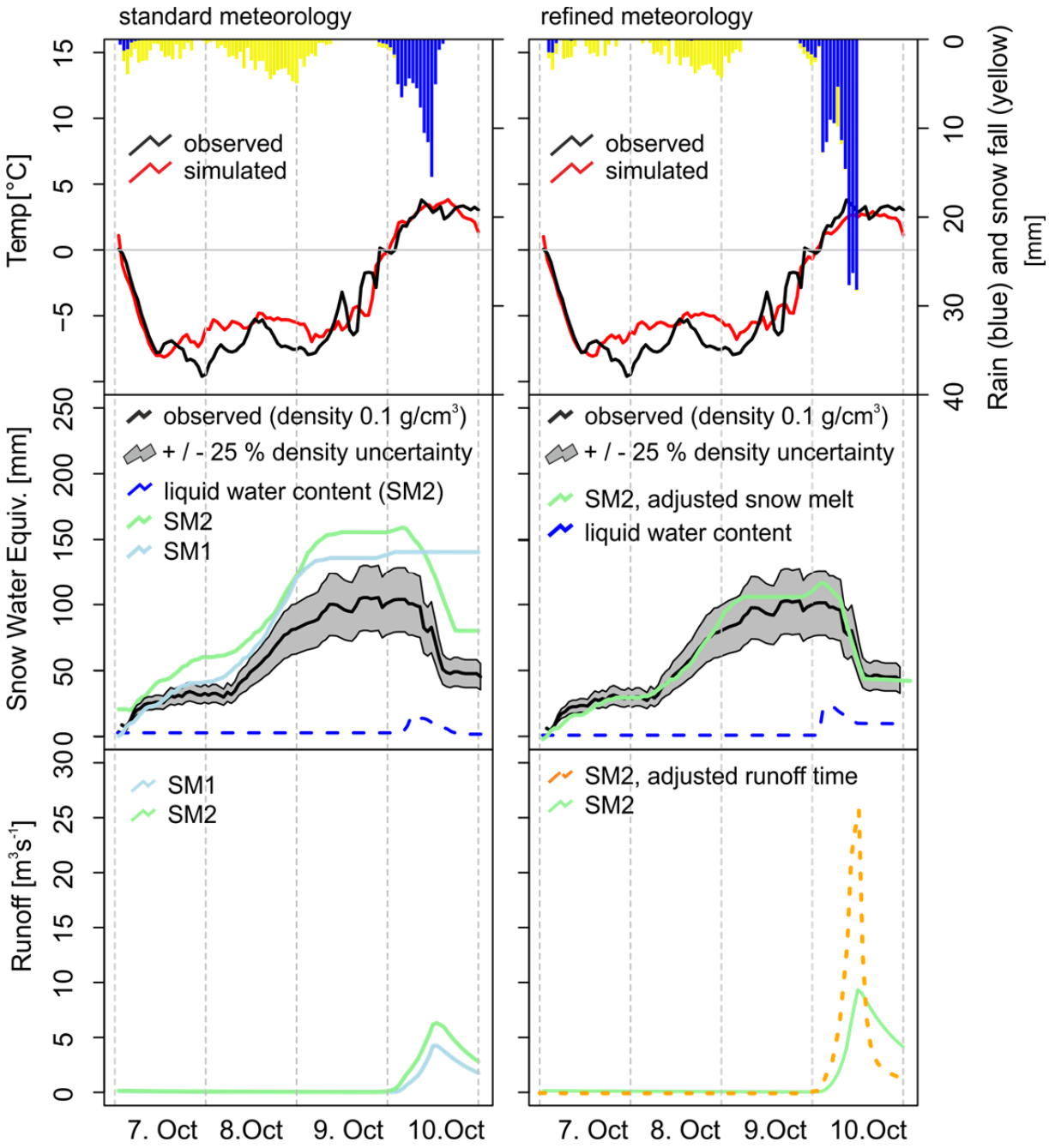

Figure 9: Model performances with standard and refined meteorology for precipitation and temperature (top row), snow depth (center row) and runoff (lower row) for the tributary river Milibach using both snow models (SM1 and SM2). Shaded grey area indicates the uncertainty origin from unknown snow density (+/- 25 % of 0.1 g/cm^3). Dashed blue line depicts the liquid water content in the snow cover. Refined meteorology and snowmelt from latent and sensible heat are able to reproduce both snow cover accumulation and depletion.

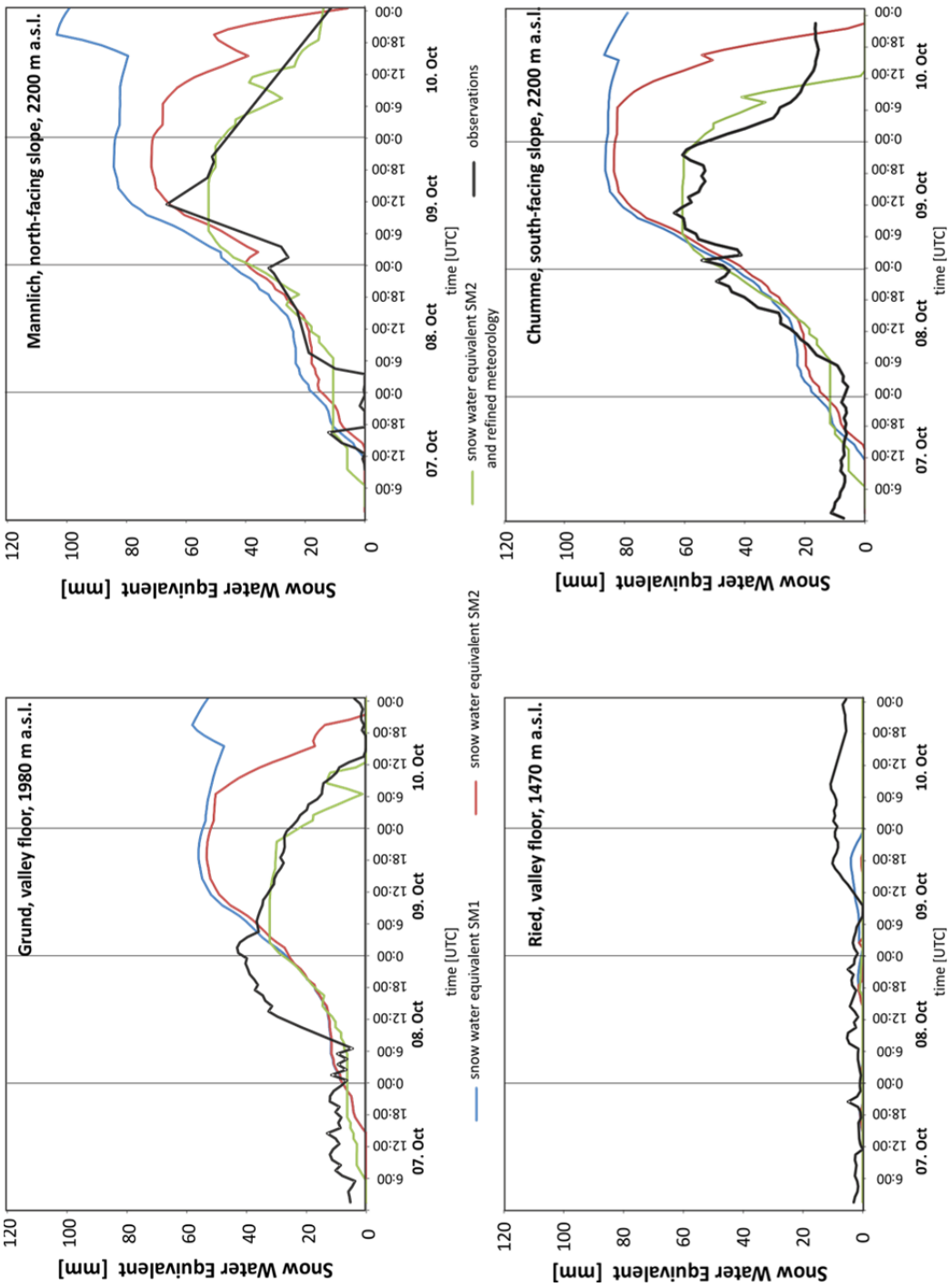

Figure 10: Snow model performance of standard (SM1, blue line), and enhanced snow modul (SM2, brown line), as well as adjusted SM2 under refined meteorology (SM2+RM, light green line) in terms of snow water equivalent (SWE) at four different meteorological stations (Reid, Grund, Mannlich, Chumme, see Figure 1) representing different altitudes and expositions. Observations (black line) are derived from snow height measurements assuming a snow density of 0.1 cm^3/g.

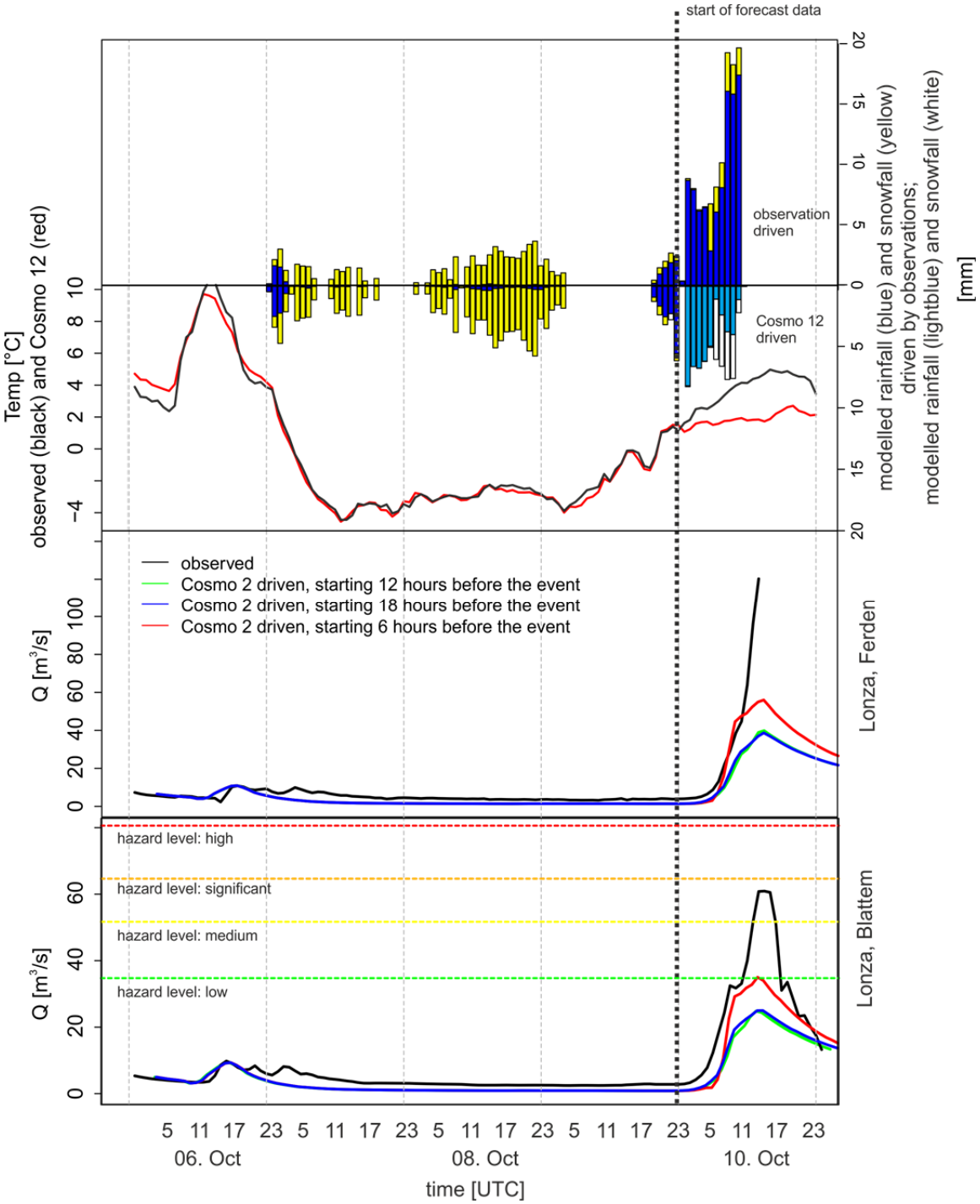

Figure 101: Simulated discharge at Lonza, Ferden and Lonza, Blatten using the best adjusted hydrological model with COSMO-2 data 6, 12, and 18 hours in advance. The temperature and the solid and liquid precipitation are average values for the entire valley taken from COSMO-2, 12 hours in advance. The blue and yellow bars and black line indicate observed rain, snow, and temperature of the refined meteorology, respectively. Hazard levels are official hazard levels corresponding to a 2-year, 10-year, 30-year, and 100-year event.